

MAR 4 1957

Copy
RM E56L07a

NACA RM E56L07a

C.1



RESEARCH MEMORANDUM

AERODYNAMIC DESIGN AND OVER-ALL PERFORMANCE OF
FIRST SPOOL OF A 24-INCH TWO-SPOOL
TRANSONIC COMPRESSOR

By James E. Hatch and Daniel T. Bernatowicz

Lewis Flight Propulsion Laboratory
Cleveland, Ohio

CLASSIFICATION CHANGED

UNCLASSIFIED

LIBRARY COPY

To

MAR 11 1957

By authority of

Nasa PA 4 *E. Hartman*
Date *3-10-59*
ND 3-19-59

LANGLEY AERONAUTICAL LABORATORY
LIBRARY, NACA
LANGLEY FIELD, VIRGINIA

CLASSIFIED DOCUMENT

This material contains information affecting the National Defense of the United States within the meaning of the espionage laws, Title 18, U.S.C., Sec. 793 and 794, the transmission or revelation of which in any manner to an unauthorized person is prohibited by law.

NATIONAL ADVISORY COMMITTEE FOR AERONAUTICS

WASHINGTON

March 4, 1957

CONFIDENTIAL
UNCLASSIFIED

UNCLASSIFIED

NASA Technical Library



3 1176 01436 5556

NACA RM E56L07a

NATIONAL ADVISORY COMMITTEE FOR AERONAUTICS

RESEARCH MEMORANDUM

AERODYNAMIC DESIGN AND OVER-ALL PERFORMANCE OF FIRST SPOOL OF
A 24-INCH TWO-SPOOL TRANSONIC COMPRESSOR

By James E. Hatch and Daniel T. Bernatowicz

SUMMARY

The two-stage first spool of a highly loaded transonic compressor was designed, built, and tested in order to investigate problems associated with a design utilizing what were considered as limiting aerodynamic parameters. The measured efficiency, weight flow, and pressure ratio were below the design values of 89.9 percent, 110 pounds per second, and 2.026, respectively. The inferior performance may be partly attributed to a combination of the following: high losses due to large rotor and stator blade root fillets, off-design operation of the second stage due to tip losses in the first-stage rotor and stator blades being higher than anticipated, and higher-than-design incidence at the hub of the first rotor due to a measured axial velocity distribution at the inlet which was different from design.

INTRODUCTION

Because future airplanes are planned to fly at higher and higher supersonic flight speeds, requirements on the compressor are becoming more severe. Problems have arisen which were either nonexistent or less acute in the subsonic region. The first of these problems is that when the compressor is operating at design mechanical speed at supersonic flight Mach numbers, it is operating at much below the design equivalent speed. For example, at a flight Mach number of 3.0 and an altitude of 35,000 feet the compressor, which is operating at constant mechanical speed, will be operating at 68.6 percent of design equivalent speed. At low altitudes the equivalent speed will be even lower. A single-spool compressor of comparable pressure ratio might be operating in the region where rotating stall would excite critical blade vibrations and result in compressor blade failure (refs. 1 to 3).

The two-spool compressor seems to offer a means of alleviating this problem because of indications that the low-pressure-ratio first spool would encounter rotating stall at a lower equivalent speed than the

~~CONFIDENTIAL~~

UNCLASSIFIED

4288

CB-1

high-pressure-ratio single-spool compressor and, therefore, avoid rotating stall over a wider speed range. In addition, the second spool is usually not required to operate at a low percentage of equivalent design speed under equilibrium operating conditions. The second problem is obtaining low specific weight. To acquire low specific weight, it is necessary to increase both mass flow per unit frontal area and stage pressure ratio, which tend to reduce weight by reducing the number of stages and maximum diameter. This combination requires high inlet axial Mach number and high tip speed, which result in a high relative Mach number on the rotor blades. The NACA five-stage transonic single-spool compressor represents such a design (ref. 4). However, the two-spool compressor offers the added desirability that the actual design tip speed of the second spool may be increased above that of the first spool because of the decreased absolute Mach number resulting from energy addition. This increased wheel speed results in an increased average stage pressure ratio for prescribed loading. The high mass flow per unit frontal area is desirable for reducing aerodynamic drag.

In order to investigate problems associated with the design of a compressor having high weight flow per unit frontal area and high stage pressure ratio commensurate with the known design limits, the NACA has designed, built, and tested the first spool of a two-spool transonic compressor. This report presents the method used in arriving at the design, some mechanical details, the over-all performance of the first spool, and some analysis of blade element loss data.

PROCEDURE

The steps taken in arriving at the first-spool design will be presented as follows in the ensuing sections of the report:

(1) First-stage design analysis: With a few exceptions, the first stage of the compressor will be the most critical from the standpoint of exceeding the design limits of such variables as rotor tip relative Mach number, rotor hub relative exit air angle, stator hub Mach number, and hub passage curvature. Consequently, to aid in selecting, within certain limits, an optimum combination of design variables for this particular compressor application, an analysis was made to determine the interrelation of the numerous design parameters. As much as possible, the design values for this first stage will be any limiting values as indicated from previous experimental results or design studies.

(2) Design procedure: The design of a compressor may be broken down into two phases: (1) determination of the design velocity diagrams of each blade row so that no known limits will be exceeded, and (2) selection of airfoil-section geometry and stacking of these sections so that the required velocity diagram at each radius will be acquired. These steps will be covered in the following sections of this report:

(a) Initial aerodynamic design approximation: For supersonic flight application an over-all compressor total-pressure ratio of approximately 7.0 was chosen. From consideration of work-load split on the two turbines, a total-pressure-ratio split of approximately 2.0 and 3.5 in the first and second spools, respectively, was chosen (ref. 5).

In this phase of the design simple radial equilibrium (no radial flow or radial gradient of entropy) and the energy and continuity equations were used to determine the air-passage contour.

(b) Final aerodynamic calculations: In this phase refinements were made to obtain the velocity diagrams including the effects of radial flow. Radial gradients of entropy in the first spool were neglected with the assumption that their effect on the axial velocity distribution in the first two stages would not be significant.

(c) Blade-section determination: The airfoil-section characteristics are presented, and the method used in stacking these sections to form the blades is outlined.

FIRST-STAGE DESIGN ANALYSIS

The first stage of the compressor is usually the most critical with respect to design limits. Consequently, before starting the design an analysis was made to determine the effect of the important design variables on the first-stage parameters to facilitate an optimum selection of design values.

In order to limit the number of design variables in the analysis the following parameters were fixed:

(1) First-rotor tip diameter. This value was set at 24 inches as a value that would give weight flows and rotative speeds commensurate with laboratory test equipment and be large enough to give adequate room for instrumentation.

(2) Hub-tip radius ratio at inlet to first-rotor blade row. It is desirable to have as low a value of this parameter as possible in order to minimize the inlet axial Mach number for a specified value of equivalent weight flow per unit frontal area. The value of 0.4 was selected as the minimum value which would allow installation of the first-spool front rotor bearing and allow ample fastening area for first-stage rotor blades without prohibitive rotor blade disk stress and root centrifugal stress.

(3) Type of velocity diagram. On the basis of simplicity of design and previous experimental results it was decided to use zero whirl at the inlet to all rotor blade rows with radially constant energy addition through all rotor blade rows. This produces a pure vortex-type whirl distribution at the inlet to all stators. Typical rotor and stator velocity diagrams are shown in figure 1.

(4) Other assumptions. The assumption in the analysis of isentropic simple radial equilibrium (no radial flow or radial gradient of entropy) along with the velocity diagram assumption resulted in an axial velocity that was constant radially at all axial stations. Consequently, in the analysis calculations it was necessary only to satisfy the continuity and energy equations. In these calculations it was assumed that the first-rotor polytropic efficiency (based on total conditions) was 92 percent. Corrections for the effect of wall boundary layers on required annulus area were applied by means of a weight-flow blockage factor of 1 percent at the inlet to the first-rotor blade row and 2 percent at the exit. The weight flow used in the calculations in satisfying continuity at these axial stations was obtained by increasing the assumed flow by the percentage of the assumed boundary-layer-blockage factor. A tip solidity of 1 was used in the calculations. As a measure of blade loading in this analysis the diffusion factor developed in reference 6 was employed. The slope of rotor tip relative total-pressure-loss coefficient for minimum loss incidence angle against diffusion factor increases sharply for diffusion factors above approximately 0.4. Therefore, a maximum value of 0.35 was set for this analysis. Standard sea-level inlet conditions were assumed in all calculations.

The curves used in this analysis are presented in figures 2 and 3 with the following selected as the independent variables: tip relative and axial Mach numbers at the inlet to the first rotor, axial velocity ratio across the first rotor, reduction in tip diameter through the blade row, and rotor tip speed.

The following table illustrates the range of variables and the figures used in the first-stage analysis:

| Figure | Rotor tip relative Mach number, $M'_{1,t}$ | Rotor inlet axial Mach number, $M_{z,1}$ | Axial velocity ratio across first rotor, $V_{z,2}/V_{z,1}$ | Tip radius at rotor exit, $r_{2,t}$ ft | Rotor tip speed, $U_{1,t}$ ft/sec | Rotor tip diffusion factor, D_t | Relative exit air angle at rotor hub $\beta'_{2,h}$ deg | Weight flow per unit frontal area, $w\sqrt{\theta}/\delta A_F$ (lb/sec) sq ft |
|--------|--|--|--|--|-----------------------------------|-----------------------------------|---|---|
| 2 | ^a 1.00-1.35 | ^a 0.5-0.7 | 1.0 | 1.0 | Variable | 0.35 | Variable | Variable |
| 3(a) | 1.188 | 0.61 | ^a 0.8 - 1.2 | 1.0 | 1100 | 0.35 | Variable | 35 |
| 3(b) | 1.188 | 0.61 | 1.0 | ^a 0.954-1.00 | 1100 | Variable | 0 | 35 |
| 3(c) | 1.188 | Variable | 1.0 | ^a 0.95-1.00 | ^a 1000-1100 | 0.35 | Variable | Variable |

^aIndependent variables.

Effect of Rotor Inlet Axial and Tip Relative Mach

Numbers on Rotor Parameters

In acquiring a combination of high mass flow and high pressure ratio with transonic rotor blade operation for a fixed value of first-rotor tip relative Mach number and inlet hub-tip radius ratio, the independent variable becomes axial Mach number, weight flow per unit frontal area, or rotor tip speed. The problem then arises of what combination of tip speed and axial Mach number should be used in the design.

Figure 2 presents the variation of rotor total-pressure ratio, tip speed, inlet axial velocity, and weight flow per unit frontal area with inlet axial Mach number for three different values of rotor tip relative Mach number. For fixed values of rotor tip diffusion factor, relative Mach number, and axial velocity ratio there is little change in total-pressure ratio by changing the inlet axial Mach number, but increases in axial Mach number naturally result in increased flow per unit frontal area. At any fixed value of axial Mach number large gains in rotor total-pressure ratio can be made by increasing the rotor tip relative Mach number by increasing wheel speed. However, at the time of this design there were no experimental results for operation of rotors having tip relative Mach numbers above approximately 1.2. Also, high rotor

and blade root stresses result from the high tip speed. Consequently, for the remaining analysis the rotor tip relative Mach number was fixed at 1.188 or the value obtained from using a tip speed of 1100 feet per second and a weight flow of 35 pounds per square foot frontal area.

Effect of Axial Velocity Ratio on First-Stage Parameters

In compressors designed for high inlet axial Mach number, to obtain high mass flow per unit frontal area, it is necessary that the exit velocity be decreased to the point where it may be diffused efficiently to an acceptable burner-inlet velocity. Axial velocity reduction may also serve to decrease the magnitude of the hub slope and curvature. Consequently, it was believed desirable to investigate the effect of axial-velocity ratio across the rotor blade row on stage parameters. Figure 3(a) presents the variation of rotor total-pressure ratio, hub radius at the rotor exit, absolute and relative exit air angles at the hub, and stator hub Mach number with axial velocity ratio for fixed values of the variables listed. Large decreases in axial velocity for the specified diffusion factor result in losses in rotor total-pressure ratio. Also, the required stator hub turning becomes excessive, and the hub relative exit air angle from the rotor becomes highly negative (turning past axial direction) with an increased possibility of choking in the rotor blade passage. Gains in total-pressure ratio may be made by increasing the axial velocity across the rotor. However, this presents problems of high stator hub Mach numbers and high hub passage slope and curvature. In addition, the axial velocity would have to be decreased greatly in later stages to reach an acceptable diffuser-inlet velocity. Consequently, from the consideration of large turning past axial, high turning at the hub of the stator, and a sacrifice in pressure ratio, it was decided to use an axial velocity ratio of 1 in the remaining analysis.

Effect of Rotor Tip Diameter Reduction Through Blade Row

The effect of reduction of the rotor tip diameter through the compressor was investigated for two reasons. First, tapering the tip reduces the magnitude of the slope and curvature of the hub streamlines in the inlet stages where they are most severe in high-pressure-ratio stages. This reduction is desirable since no experimentally proven method is available of accurately accounting for the effect of large slope and curvature upon the radial distributions of axial velocity. Second, the exit diffuser can be made symmetrical without increasing the diffuser-exit diameter beyond the frontal diameter of the compressor. The symmetrical diffuser is desirable because of the shorter length possible for efficient diffusion.

4288

Figure 3(b) presents the variation of rotor total-pressure ratio, hub radius at the rotor exit, Mach number at the hub of the first stator, absolute air angle at the hub at the stator inlet (which is the same as the stator hub turning angle), and rotor tip diffusion factor with tip radius leaving the rotor. The relative air angle leaving the rotor at the hub was limited to zero since turning beyond this point would result in high turning at the hub and increased danger of choking inside the blade row. The axial velocity ratio across the blade row was fixed at 1. The other constants in the calculation are indicated in figure 3(b). The three calculation points on the figure represent the amount of reduction of the tip diameter which results in constant tip, mean, and hub radii across the blade row. All parameters are reduced by a decrease in tip diameter. A large reduction in tip radius results in a sizable reduction in rotor pressure ratio and an attendant reduction in pressure ratio in the following stages of this spool. Figure 4 illustrates the relative magnitudes of the hub passage slope and curvature for the cases shown. Blade chord was determined from the assumed tip solidity of 1 and the maximum number of blades permissible without excessive root stress. The axial chord was then determined by estimating blade setting angles. It was felt that limiting the rotor hub relative exit angle to axial was a rather severe restriction. Therefore, for the remainder of the analysis the rotor work will be limited by fixing the rotor tip diffusion factor at 0.35. Tapering the tip only through the rotor blade to a radius of 0.98 foot (11.76 in.) at the exit with the constant tip diffusion factor of 0.35 resulted in considerable reduction of the hub slope and curvature with a reduction in rotor total-pressure ratio from 1.444 to 1.399. Further reduction in the tip radius through the stator with constant axial velocity across the stator resulted in a large decrease in hub radius through the stator because of the relatively low static-pressure rise in the stator for this type of velocity diagram. Therefore, tapering only the tip over the first rotor gives a smooth hub shape without resorting to axial velocity increases across the stator. It was decided to investigate the effect of tapering the rotor tip diameters on stage parameters while maintaining a constant tip diffusion factor of 0.35.

Effect of Rotor Tip Speed and Exit Radius

An investigation was made to determine the effect on first-stage parameters of varying the tip speed as well as the exit tip radius. For these calculations tip speeds of 1100, 1050, and 1000 feet per second at the rotor inlet were used and the effect of rotor exit tip radius was investigated for each speed. The rotor inlet tip relative Mach number was maintained at 1.188, which is the value arising from a weight flow of 35 pounds per square foot of frontal area and a tip speed of 1100 feet per second. The flow was allowed to vary at other speeds to maintain the same relative Mach number.

Figure 3(c) presents the variation of total-pressure ratio, radius and air angle at the hub at the rotor exit, relative air angle at the exit from the rotor at the hub, and stator hub Mach number with rotor exit tip radius for the three different tip speeds. Under the conditions of the calculations total-pressure ratio and rotor exit hub radius are not greatly affected by changes in rotor tip speed. Decreasing the tip speed increases the stator hub Mach number and at 1000 feet per second the Mach number approaches 1. A reduction in tip speed also results in high negative values of rotor relative exit angle at the hub at a tip speed of 1000 feet per second with attendant danger of choking in the rotor passage. The stator hub absolute air angle decreases with decreased tip speed, which alleviates the required turning through the stator.

Summary of Results of Design Analysis

After consideration of the effect of rotor tip exit radius as presented in figures 3(b), 3(c), and 4 it was decided to reduce the tip radius at the exit of the first rotor to 0.98 foot and maintain it constant through the remainder of the compressor. Based on figures 2, 3(a), and 3(c) the first-rotor tip speed of 1100 feet per second and weight flow per unit frontal area of 35 were selected as offering the best compromise after consideration of blade root and rotor centrifugal stresses, stator hub Mach number and turning angle, rotor hub relative exit air angle, and rotor tip inlet relative Mach number. Analysis of figure 3(a) led to the selection of an axial velocity ratio of 1.0 across the first rotor. An axial velocity ratio near 1.0 gives a good compromise between stator hub Mach number, turning angle, and rotor hub exit relative air angle. These factors become less critical in later stages because of higher stagnation temperatures and larger hub radii. Also, it was anticipated that the rotor tip diffusion factor could be increased in the later stages, resulting in a higher over-all pressure ratio for a given number of stages. Axial velocity could be decreased in these later stages. The first-rotor total-pressure ratio for the above conditions is 1.40. A preliminary calculation indicated the need of only two stages in the first spool for a pressure ratio of 2.0.

DESIGN PROCEDURE

Initial Design Assumptions

In the design of the first spool a number of initial assumptions were made which were based on information obtained from other single- and multistage experimental results and on the results of the first-stage analysis. The initial assumptions were necessary in order to fix the stage energy addition, total-pressure ratio, and hub profile shape before proceeding with refinements in the compressor design. The itemized initial assumptions are as follows:

(1) Boundary-layer-blockage allowance. A blockage allowance of 1 percent was assumed at the inlet to the first rotor with an increase of 1 percent through each blade row of the first spool. This allowance was applied as a flow deficit in satisfying continuity, that is,

$$w_c = \frac{w_{\text{design}}}{1 - \text{boundary-layer blockage}}$$

(All symbols are defined in appendix A.)

(2) The initial assumption of the rotor tip diffusion factor was 0.35 and 0.415 in the first and second rotors, respectively. The rotor hub diffusion factor limit was placed at approximately 0.55 if this limit was reached before the previously mentioned tip limits. The diffusion factor limit on all stators was placed at approximately 0.55 at all radii based on the results of reference 6.

(3) The axial velocity was assumed constant across all blade rows in the first spool.

(4) No whirl component of velocity entering rotor blade rows existed.

(5) Constant energy addition existed at all radii in the rotor blade rows. Assumptions 4 and 5 result in a vortex-type whirl distribution downstream of all rotor blade rows.

(6) The rotor polytropic efficiency was assumed to be 92 and 91 percent in the first and second rotors, respectively, and was assumed constant radially. In this case the polytropic efficiency is based on stagnation conditions, that is, $P_2/P_1 = (T_2/T_1)^{m/m-1}$, and so forth, where

$$m = \frac{\eta_p}{\eta_p - \frac{\gamma}{\gamma-1}}$$

(7) The total-pressure loss across stationary blade rows in terms of a loss coefficient was assumed to be 0.015 at all radii:

$$\bar{w} = \frac{\Delta P}{\frac{1}{2} \rho_1 V_1^2} = 0.015$$

(8) The tip solidity was 1.0 for all blade rows.

It was the aim in this design to incorporate, to the extent of available information, all factors which influence the velocity diagrams at each blade element on the streamline path through the machine. This involves satisfying the exact equations of energy, continuity, state, and momentum simultaneously and is obviously a rather difficult task. For example, the magnitude of the radial flow term in the equilibrium equation that influences the radial distribution of axial velocity in a

design depends, to a large extent, upon the contour of the compressor hub (ref. 7), which depends upon satisfying the energy and continuity relations. Satisfying continuity, in turn, depends upon the axial velocity distribution. The approach taken was to determine a hub contour by using simple radial equilibrium and then recompute the velocity diagrams using the complete radial equilibrium equation.

Initial Aerodynamic Design Approximation

From equation (3a) of reference 7 the equation for radial equilibrium, assuming axisymmetric flow with zero local viscous forces, is

$$c_p \frac{\partial T}{\partial r} = t \frac{\partial S}{\partial r} + V_\theta \frac{\partial V_\theta}{\partial r} + \frac{V_\theta^2}{r} + V_z \frac{\partial V_z}{\partial r} - V_z \frac{\partial V_r}{\partial z} \quad (1)$$

For the initial step in this design it was assumed that the radial gradient of entropy and the radial flow term (first and last terms on right) were negligible after all blade rows. This assumption, together with the previous assumption of whirl distribution and the stipulation of radially constant energy addition through rotor blade rows, results in radially constant axial velocity after all blade rows. The approximate solution facilitates the determination of annulus areas after all blade rows. The method of solution was as outlined in the following steps:

(1) For the first-rotor blade row of the first spool the preliminary analysis showed that a constant tip diameter through the blade row resulted in high hub taper with attendant high hub curvature. Therefore, it was decided to reduce this effect with a reduction in tip diameter through the rotor. Therefore, for any ratio of inlet-to-exit tip diameter the tip speed ratio $U_{1,t}/U_{2,t}$ was determined. This value, together with the design tip speed at the first-rotor inlet, solidity, axial velocity ratio, and diffusion factor as given above, was used in equation (B6) of appendix B to determine the rotor energy addition. Equation (B3) was then used to determine the tip whirl component of velocity downstream of the rotor blade row. Since a vortex-type whirl distribution exists at this station, the whirl component at any radius is determined. By use of the boundary-layer-blockage correction, axial velocity, and rotor polytropic efficiency, the hub radius required to satisfy continuity after the rotor blade row could then be ascertained.

The annulus area required to satisfy continuity downstream of the first-stage stator was determined by use of the assumed stator loss coefficient, boundary-layer-blockage correction, axial velocity, and the fact that the flow was axial at the station and that the tip diameter was constant through the blade row.

(2) The tip diameter was held constant for the second stage in the first spool. Consequently, for the second-rotor blade row equation (B7) was then used with the axial velocity ratio, rotor tip diffusion factor, design tip speed, and solidity to obtain the design stage total-temperature rise. Equation (B3) was again used to determine the tip whirl component, and the whirl at any radius was known from the vortex distribution. The hub radius required after the rotor to satisfy continuity was determined in the same manner as in step (1).

The annulus area required to satisfy continuity after the second stator was again determined by use of the stator pressure loss coefficient, boundary-layer-blockage correction, axial velocity, and the fact that the flow was axial and the tip diameter was constant.

(3) Before proceeding further it was necessary to make sure that the rotor hub and stator diffusion factor limits (approx. 0.55) were not exceeded. If the limits were exceeded it was necessary to either increase the solidity or reduce the design tip diffusion factor on the rotor. The latter would serve to reduce the rotor hub diffusion factor and the diffusion factor at all radii on the succeeding stator.

(4) The hub and tip contours were then determined throughout the compressor. In order to ascertain the hub shape, it was necessary to compute the blade chords. This was done for the first-rotor blade row by selecting the maximum number of blades which could be used without resulting in excessively high centrifugal stresses in the rotor and blade root. The nearest prime number below this value was selected to minimize the possibility of preceding strut wakes exciting the blades at their natural frequencies. Once the number of blades was determined the tip chord could be found since the tip diameter and solidity were known. The chord (on cylindrical surfaces) was held constant over the whole blade span. For the next rotor the number of blades was increased slightly over the first rotor to cut down the required axial length. This was possible since the hub radius was increasing and the blade span was decreasing and tending to relieve the stress situation. Again, care was taken to select the number so that it was not the same as upstream and downstream rotors or stators. The chord, which was held constant radially, was computed by the same procedure used in the preceding blade row. The blade setting angle at the hub and tip radii for all blade rows in the first spool was approximated so that the axial length of the blade rows could be determined. Approximately 1/2-inch minimum clearance was allowed between each blade row for instrumentation purposes. A plot of the passage contour was then made as indicated by the points on figure 5. Since the calculated points resulted in an uneven hub, the hub was faired as shown.

(5) The faired hub resulted in passage areas entering some blade rows which were different from that area for the prescribed axial velocity. Consequently, it was necessary to compute the new axial velocity which would satisfy continuity with the same energy addition through each blade row (same tip tangential velocity component). After computing the new velocities and state functions it was necessary to determine if any diffusion factor limits were exceeded, in which case it was necessary to increase the solidity by adding blades.

Final Aerodynamic Design Calculations

With the passage contour determined the next step was to refine the design by taking into account the effect of the radial flow and entropy terms in the radial equilibrium expression (eq. (1)) at the axial stations where the terms were significant. In a design of this type there is little shift of the streamlines through the blade rows because of redistribution of mass flow alone compared with a symmetrical diagram design with constant energy addition (ref. 8). Consequently, the radial flow term is mainly a function of the contour of the hub. In the first spool the hub first and second derivatives (dr/dz and d^2r/dz^2 , respectively) are high, and, as a result, the radial flow term was included in the calculations for the axial velocity distribution after the blade rows in this spool.

Entropy gradient. - It was assumed that losses would be essentially constant with radius in the inlet stages if optimum incidence angles could be achieved at all radii (ref. 7). Therefore, the design polytropic efficiency was assumed to be constant radially through both rotor blade rows in the first spool, and because the radial gradient of loss through the stators was small (because of assumed constant loss coefficient), it was unnecessary to account for the effect of entropy upon velocity distribution in the first spool.

Correction for radial flow. - In accounting for the effect of radial flow upon axial velocity distribution at the axial stations between blade rows it was stipulated that, for the final distribution of axial velocity, the energy addition be of the same magnitude as that determined in the section "Initial Aerodynamic Design Approximation" and be constant radially. There was zero whirl velocity entering each rotor blade row. As a result, the whirl component leaving all rotor blade rows had a vortex distribution. In view of the foregoing and the fact that the radial gradient of entropy was assumed to be negligible in the first spool, equation (1) can be written as:

$$V_z \frac{\partial V_z}{\partial r} = V_z \frac{\partial V_r}{\partial z} \quad (2)$$

4288

In order to facilitate calculation of the radial distribution of axial velocity after blade rows, it was desired to obtain an expression for axial velocity at any radius as a function of only the streamline geometry and Mach number. This derivation will be found in appendix C. From equation (C5) it is seen that a solution for velocity distribution after any blade row could be obtained if the contours of all streamlines on the r, z surface at the axial calculation station were known (fig. 6). The boundary conditions are known since the hub and tip streamlines must follow the hub and tip contours. As an initial calculation the mass-flow distribution from the initial design approximation was used to determine the boundaries of 10 stream tubes after each blade row. Smooth streamlines were then drawn through these points. The resulting first and second derivatives were used in equation (C5) together with the Mach number from the initial design approximation to obtain a new distribution of axial velocity. The result from this equation was in the form of an axial velocity ratio from one streamline to the next. These ratios were used together with continuity, state, and Mach number relations to get the absolute value of the velocity at each radii. The resulting mass-flow distribution was used to obtain the boundaries of a new set of stream tubes, and an adjusted set of streamlines was drawn. This second trial indicated that a good approximation would be to assume linear variation of first and second derivatives from the value at the hub to zero at a point 25 percent of the passage height from the tip after all blade rows in the first spool. At the inlet to the first spool the hub and tip contours were made straight lines for some distance upstream of the first-rotor blade row in an attempt to minimize the gradient of axial velocity at the inlet. A linear distribution of first derivative from hub to tip was used at this station. Unpublished data on single-stage tests have verified that the above method provided satisfactory agreement with measured results. For expediency no attempt was made at any station to correct the axial velocity distribution for the effect of blade-thickness taper (ref. 9). It was felt that this effect would, to some degree, be compensated for by determining the optimum incidence from rules based on experimental data.

With the above selected distributions of first and second derivatives of streamlines at each axial station, calculations were made of velocity distributions (eq. (C5)) which satisfied continuity at axial stations approximately midway between blade rows. The energy addition was constant and of the magnitude determined in the section "Initial Aerodynamic Design Approximation". The distributions of axial velocity at the inlet and exit of all blade rows throughout the first spool were computed and are presented in figures 7(a) through (c). The values of hub and tip streamline first and second derivatives at the calculation station are shown on the figures. It was then necessary to compute the diffusion factor of all blade rows and, if any design limits were exceeded because of the effect of radial flow correction, the diffusion factor was reduced by adding blades (eq. (B1)).

Final Design Information and Velocity Diagrams

After the axial velocity distributions and hub radii were calculated at all axial stations it was possible to calculate the design speed performance information and velocity diagrams. Some of the final design information is tabulated as follows:

| | |
|---|-------|
| Total-pressure ratio (two stages) | 2.026 |
| Adiabatic efficiency, percent | 89.9 |
| Equivalent weight flow, lb/sec | 110 |
| Equivalent tip speed, ft/sec: | |
| Inlet to first-rotor blade | 1100 |
| Second-rotor blade | 1078 |
| Tip diameter, in.: | |
| Inlet to first-rotor blade | 24.00 |
| Remaining blade rows | 23.52 |
| Axial length (first-rotor inlet to second-stator exit), in. | 9.2 |
| Hub-tip radius ratio: | |
| Inlet to first rotor | 0.400 |
| Exit from second stator | 0.647 |

The design total pressure and total temperature at all axial stations for standard sea-level inlet conditions are presented in table I.

The chords (on cylindrical surfaces) of all blade rows were constant with radius. The number of blades in each row with their chords and solidity are given in table II. The solidity was computed by using the chord on the cone obtained by connecting the inlet and exit calculation radii, and the spacing was obtained by using the mean of these radii.

Since the distributions of axial velocity, whirl, and streamline slope were known at each axial and radial station, it was possible to compute all relative and absolute velocities, angles, and Mach numbers. The resultant velocity at all axial stations in the first spool was the vectorial addition of axial, whirl, and radial components of velocity. The resultant of the three components was used to determine the absolute and relative velocities, air angles, Mach number, and diffusion factor. The design distribution of air angles, Mach number, and diffusion factor will be found in figures 8(a) through (d). The Mach number variation at the inlet to the compressor is presented in figure 9.

With the velocity diagram information determined, the next problem was to select the blading that would give the required turning at each section with a minimum of loss at the design condition.

Blade-Section Determination

The final phase of the design was concerned with selecting the airfoil at each radial element which would give the required turning at a

minimum loss for the particular design value of Mach number, air stagger angle, and solidity. An analysis on high Mach number blade sections (ref. 10) indicates that for rotors operating in this tip Mach number range (1.0 to 1.2) a double-circular-arc airfoil section (circular-arc pressure and suction surfaces) is the optimum geometrical shape. Also, since the first two stators are operating at hub Mach numbers of 0.8 or over, it was decided to use double-circular-arc stators throughout.

From figure 10 it can be seen that the following equations may be written by consideration of the blade-section geometry and air velocities relative to the blade section:

$$\beta'_1 = \lambda + \frac{\phi}{2} + i \quad (3)$$

$$\lambda = \frac{\phi}{2} - \delta^\circ + \beta'_2 \quad (4)$$

Combining equations (3) and (4) yields

$$\beta'_1 - \beta'_2 = \Delta\beta' = \phi + i - \delta^\circ \quad (5)$$

From equation (5) it can be seen that the desired design turning for any section can be obtained with various combinations of camber angle ϕ and incidence angle i . The problem is determining the minimum loss angle of incidence for the section Mach number, camber angle, solidity, and inlet air angle. The method of computing the minimum loss incidence angle and deviation angle is presented in reference 11. In all blade rows through the first spool the inlet and exit air angles and Mach numbers presented in figures 8 and 9 include axial, radial, and tangential velocity components. In the determination of airfoil-section characteristics, the inlet and exit angles and velocities were transformed from α_1 and α_2 to α , which is the semicone angle between the two calculation stations z_1 and z_2 (fig. 11). The double-circular-arc airfoil section was wrapped around the surface of this cone.

The airfoil-section characteristics of camber angle, blade setting angle, incidence and deviation angle together with semicone angle are plotted against inlet radius in figure 12.

MECHANICAL CONFIGURATION

Figure 13(a) illustrates some of the mechanical details of the first-spool construction. Both stator blade rows were shrouded at the hub for the purpose of reducing the magnitude of possible vibratory stresses. However, it was contemplated that a modification to unshrouded stators might be made to determine the effect of shrouded stators. With this

in mind, large stator blade root fillets were incorporated. These fillets consisted of a 3/16-inch radius at the root blended into a parabolic fairing such that the fillet extended out 1/2 inch on the blade surface. The labyrinth seal on the first-stator shroud prevented recirculation around the shroud.

Figure 13(b) shows leading- and trailing-edge views of the fillet area of a stator blade. The cutout shown on the center photograph is to relieve the stress at the junction between the base and blade where past experience has shown cracks to start. The stator blade thickness-to-chord ratio was 5 and 10 percent at the hub and tip, respectively. The thickness was varied linearly with radius. The leading- and trailing-edge radii were 0.010 inch.

Figure 13(c) shows the leading and trailing edges of a rotor blade. The fillets at the hub of the rotors were of the same type as the stator fillets described above. The root fastening was a cylindrical-type bulb. The flat area on the bottom of the bulb allows use of 0.040-inch metal strips for retaining the blade in the axial direction. The rotor blade thickness-to-chord ratio was 10 and 6 percent at the hub and tip, respectively. A linear variation of thickness with radius was used. The leading- and trailing-edge radii were 0.010 inch. The thick tip section was used to reduce the danger of breakage of blade corners.

During tests of the first spool alone a wooden hub fairing piece was attached downstream of the center bearing housing (right side of fig. 13(a)) to diffuse the flow to low velocity before entering the exit pipe.

OVER-ALL PERFORMANCE

The over-all performance of the first spool is presented in figure 14. Inlet stagnation conditions to the compressor were measured by 10 total-pressure and 10 total-temperature probes in the inlet depression tank. Exit stagnation conditions were measured by means of a combination total-pressure and spike-type total-temperature probe. The probe was used to survey 25 circumferential positions at each of five radial positions so that it covered one complete passage of the second-stage stator. Weight flow was measured with an adjustable orifice. The peak adiabatic efficiency value of 85 percent occurred at 80 percent of equivalent design speed. However, the peak efficiency at all other speeds was within three points of this value. The peak efficiency of 82.5 percent at design speed was 7.4 points below the design value. The choke flow at design speed is approximately 105 pounds per second. This flow would be approximately 2 percent higher if the pressure drop across the inlet struts were taken into account. The pressure ratio at the stall limit at design speed was 1.92. The peak-pressure-ratio point at 110 percent speed is only approximate because of a mechanical failure which occurred before

complete data could be taken. No rotating stall was encountered at any speed, and the blade vibratory stresses were very low. The blade rows probably exhibit the abrupt type of stall characteristic described in reference 12, which leads, in this case, to complete compressor stall.

Preliminary analysis of the blade-element performance, which was taken at the same time as the over-all performance, indicates that considerable loss in total pressure occurred across the large fillets employed at the tip of the stator blades. The radial variation of stator loss coefficient for the first- and second-stator blade rows is presented in figure 15 for the intermediate flow point at design speed. The stator loss coefficient was based on the total-pressure loss between the value at the inlet and the circumferentially integrated total pressure at the exit. The stator loss coefficient was also computed using the difference between the downstream free-stream and integrated total pressures. This loss coefficient showed the same trends. A high loss at the tip of the first stator is indicated in figure 15(a). The outer measuring station after the stator is 0.45 inch from the tip and the fillet extends out 0.5 inch on the blade. Figure 15(b) indicates a high loss region at both hub and tip. The outer measuring station after this stator row is 0.35 inch from the outer casing. The high loss at the hub of the stator may be due to increased secondary-flow losses resulting from the use of stator shrouds. The circumferential variation of total pressure at the five radial measuring stations after the first- and second-stator blade rows is presented in figure 16. The wakes at tip and hub after both stators are wider than at the other radii.

Figure 17(a) presents the radial variation of first-rotor efficiency and total-temperature and total-pressure ratios for the intermediate flow point at design speed. It can be seen that the first-rotor efficiency drops off in the tip region. On the basis of this data the assumption of no entropy gradient radially was not a good one. This could be partially due to not attaining design flow with resultant off-design incidence. It has been shown that for tip relative Mach numbers of about 1.2 there are shock and core losses (refs. 13 to 15) which can be of greater magnitude than realized at the time this compressor was designed. The magnitude of shock losses is a function of suction surface Mach number, which is dependent on blade-section incidence, camber, and thickness for a prescribed inlet relative Mach number. The shock losses could account for much of the decreased efficiency near the tip of the first rotor. These losses were probably aggravated by use of the 6-percent-thick tip section. Also presented in figure 17(a) are the radial variations of total-pressure and total-temperature ratios across the first rotor.

Figure 17(b) presents the radial variations of second-rotor efficiency and total-pressure and total-temperature ratios after the second rotor. The tip efficiency of this rotor is very low and can be attributed

to off-design incidence brought about by the tip losses in the first rotor and stator and to possible shock losses in the second rotor.

A comparison of design with measured values of axial velocity and incidence at the inlet to the first rotor is presented in figure 18. The measured incidence values were adjusted to account for the fact that the measuring station was approximately 1 inch ahead of the first rotor where the flow area was considerably larger than at the inlet to the rotor. The incidence angle at the hub of the rotor was higher than design because the axial velocity at the hub was lower than design. This discrepancy could have been partially due to choking near the hub of the rotor resulting from the large rotor blade fillets. Also, the assumption that, because the outer and inner walls at the inlet to the rotor had no curvature, the streamlines all across the passage had no curvature is not valid. The high rotor hub incidence may have been instrumental in causing a total span stall of the blades and complete compressor stall rather than a rotating stall. The decrease in efficiency toward the hub of the first rotor indicated in figure 17(a) could be due to this high incidence angle.

CONCLUDING REMARKS

A highly loaded two-stage transonic first spool for a two-spool compressor was designed, built, and tested, and the following concluding remarks can be made:

1. The design pressure ratio, weight flow, and adiabatic efficiency were 2.026, 110 pounds per second, and 89.9 percent, respectively.

2. The measured stall-limited pressure ratio at design speed was 1.92. The choke flow at design speed was 105 pounds per second. Peak measured adiabatic efficiency at design speed was 82.5 percent.

3. The failure to meet design conditions may be attributed to the following:

(a) The low peak efficiency at all speeds indicates that the loss due to large fillets at the rotor and stator blade roots probably had considerable influence on the performance. Shrouded stators may have increased the secondary-flow losses in the hub region.

(b) The low tip region efficiency of the second rotor could be attributed partially to off-design incidence brought about by tip losses in the first-rotor and -stator blade rows.

(c) Higher-than-design incidence at the hub of the first rotor due to the fact that measured axial velocity distribution at the inlet was different from design may have been detrimental to the performance.

Lewis Flight Propulsion Laboratory
National Advisory Committee for Aeronautics
Cleveland, Ohio, December 7, 1956

4288

CB-3 back

APPENDIX A

SYMBOLS

| | |
|-------------------------------------|---|
| A | flow area perpendicular to axis, sq ft |
| a | velocity of sound, ft/sec |
| c_p | specific heat at constant pressure, ft-lb/(slug)(°R), equal to Jgc_p in engineering units |
| D | diffusion factor (ref. 6) |
| g | acceleration due to gravity, ft/sec ² |
| i | incidence angle, deg |
| J | mechanical equivalent of heat, ft-lb/Btu |
| M | Mach number |
| m | polytropic exponent |
| P | total pressure, lb/sq ft |
| R | gas constant; ft-lb/(slug)(°R), equal to gR in engineering units |
| r | radius, ft |
| S | entropy, lb-ft/(slug)(°R), equal to gS in engineering units |
| T | total temperature, °R |
| t | static temperature, °R |
| U | rotor velocity, ft/sec |
| V | gas velocity, ft/sec |
| w | weight flow, lb/sec |
| $\frac{w\sqrt{\theta}}{\delta A_F}$ | equivalent weight flow per unit frontal area, lb/sec-ft ² |
| z | axial distance, ft |

| | |
|----------------|---|
| α | angle between streamline and axial direction, deg $\left(\tan^{-1} \frac{dr}{dz}\right)$ |
| β | angle between air velocity and axial direction, deg |
| γ | ratio of specific heats |
| δ | ratio of inlet total pressure to NACA standard sea-level pressure of 2116 lb/sq ft |
| δ° | deviation angle, deg |
| η | adiabatic efficiency |
| η_p | polytropic efficiency |
| θ | ratio of inlet total temperature to NACA standard sea-level temperature of 518.7° R |
| λ | blade setting angle, deg |
| ρ | static density, slug/cu ft |
| σ | solidity |
| ϕ | blade camber angle, deg |
| $\bar{\omega}$ | total-pressure-loss coefficient, $\bar{\omega} = \frac{\Delta P}{\frac{1}{2} \rho_1 V_1^2}$ |

Subscripts:

| | |
|---|---|
| a | based on stagnation conditions |
| c | continuity |
| F | frontal |
| h | hub |
| k | radial station where variables are known or assumed |
| m | mean |
| r | radial direction |
| t | tip |

- u radial station where some variables are unknown
- z axial direction
- θ tangential direction
- 1 axial station at inlet to blade row or inlet to first rotor
- 2 axial station at exit from blade row or exit from first rotor
- 3 axial station at exit from first stator
- 4 axial station at exit from second rotor
- 5 axial station at exit from second stator

Superscript:

- ' relative to rotor blade row

APPENDIX B

DERIVATION OF EXPRESSIONS FOR DETERMINING STAGE TOTAL-TEMPERATURE
RISE, TOTAL-PRESSURE RATIO, AND STATIC-TO-TOTAL RATIOS

The expression of the diffusion factor from reference 6 is

$$D = 1 - \frac{V_2'}{V_1'} + \frac{\Delta V_{\theta}'}{2\sigma V_1'} \quad (B1)$$

By applying this equation to the rotor blade tip section the following substitution may be made for the type of velocity diagram used in this design:

$$\Delta V_{\theta,t}' = U_{1,t} - U_{2,t} + V_{\theta,2,t} = U_{1,t} - U_{2,t} + \Delta V_{\theta,t} \quad (B2)$$

$$\Delta T_t = \frac{U_{2,t} V_{\theta,2,t} - U_{1,t} V_{\theta,1,t}}{c_p}$$

or, for this particular design

$$\Delta T = \frac{U_{2,t} V_{\theta,2,t}}{c_p} = \frac{U_{2,t} \Delta V_{\theta,t}}{c_p} \quad (B3)$$

$$V_{2,t}' = \sqrt{(U_{2,t} - V_{\theta,2,t})^2 + V_{z,2}^2} \quad (B4)$$

Substituting equations (B2) and (B4) into (B1), squaring, dividing by $U_{2,t}^2$, and collecting the coefficients of the $V_{\theta,2,t}$ terms yields

$$\left(1 - \frac{1}{4\sigma_t^2}\right) \frac{V_{\theta,2,t}^2}{U_{2,t}^2} - \left[2 + \frac{V_{1,t}'}{U_{2,t}} \frac{(1 - D_t)}{\sigma_t} + \frac{\left(\frac{U_{1,t}}{U_{2,t}} - 1\right)}{2\sigma_t^2}\right] \frac{V_{\theta,2,t}}{U_{2,t}} + \left[1 + \left(\frac{V_{z,2}}{U_{2,t}}\right)^2 - \left(\frac{V_{1,t}'}{U_{2,t}}\right)^2 (1 - D_t)^2 - \frac{V_{1,t}'}{U_{2,t}} \frac{\left(\frac{U_{1,t}}{U_{2,t}} - 1\right)(1 - D_t)}{\sigma_t} - \frac{\left(\frac{U_{1,t}}{U_{2,t}} - 1\right)^2}{4\sigma_t^2}\right] = 0 \quad (B5)$$

By substituting $V_{\theta,2,t}$ from equation (B3) into equation (B5) the following equation is obtained:

$$\left(1 - \frac{1}{4\sigma_t^2}\right) \left(\frac{c_p \Delta T}{U_{2,t}^2}\right)^2 - \left[2 + \frac{V_{1,t}' (1 - D_t)}{U_{2,t} \sigma_t} + \frac{\left(\frac{U_{1,t}}{U_{2,t}} - 1\right)}{2\sigma_t^2}\right] \frac{c_p \Delta T}{U_{2,t}^2} + \left[1 + \left(\frac{V_{z,2}}{U_{2,t}}\right)^2 - \left(\frac{V_{1,t}'}{U_{2,t}}\right)^2 (1 - D_t)^2 - \frac{V_{1,t}' \left(\frac{U_{1,t}}{U_{2,t}} - 1\right) (1 - D_t)}{U_{2,t} \sigma_t} - \frac{\left(\frac{U_{1,t}}{U_{2,t}} - 1\right)^2}{4\sigma_t^2}\right] = 0 \quad (B6)$$

Equation (B6) can then be solved by the quadratic formula, in which case the radical is prefixed with the negative sign.

For the special case where $U_{1,2} = U_{2,t}$ equation (B6) reduces to

$$\left(1 - \frac{1}{4\sigma_t^2}\right) \left(\frac{c_p \Delta T}{U_{2,t}^2}\right)^2 - \left[2 + \frac{V_{1,t}' (1 - D_t)}{U_{2,t} \sigma_t}\right] \frac{c_p \Delta T}{U_{2,t}^2} + \left[1 + \left(\frac{V_{z,2}}{U_{2,t}}\right)^2 - \left(\frac{V_{1,t}'}{U_{2,t}}\right)^2 (1 - D_t)^2\right] = 0 \quad (B7)$$

The rotor total-temperature rise was determined once equations (B6) or (B7) were solved since $U_{2,t}$ and c_p were known. Also, the whirl at any radius could be determined from equation (B3) and the vortex distribution. The rotor total-pressure ratio was then found by the following relation:

$$\frac{P_2}{P_1} = \left(\frac{\Delta T}{T_1} + 1\right)^{\frac{m}{m-1}} \quad (B9)$$

where

$$m = \frac{\eta_p}{\eta_p - \frac{\gamma - 1}{\gamma}}$$

and also

$$\frac{\rho_{2,a}}{\rho_{1,a}} = \left(\frac{\Delta T}{T_1} + 1 \right)^{\frac{1}{m-1}} \quad (B10)$$

The static-to-total ratios at any station were determined by computing $V/a_a = V/\sqrt{\gamma RT}$ and using reference 16, where the absolute velocity was determined from the known whirl velocity and the axial velocity as computed by the method of appendix C. For first-spool calculations the value of c_p was held constant at the value obtained from reference 17 for standard sea-level temperature (518.7° R). The value of γ used in determining the total-pressure ratio and the stagnation velocity of sound was taken as 1.4.

#488

CB-4

APPENDIX C

DERIVATION OF EXPRESSION FOR CORRECTING AXIAL VELOCITY

DISTRIBUTION FOR THE EFFECT OF RADIAL FLOW

By considering the differentiation of equation (2) to take place along the streamline, the equation may be written as

$$\frac{\partial V_z}{\partial r} = \frac{\partial V_r}{\partial z} = \frac{\partial V_z}{\partial z} \frac{dr}{dz} + V_z \frac{\partial}{\partial z} \left(\frac{dr}{dz} \right)$$

or

$$\frac{\partial V_z}{\partial r} = \frac{\frac{dV_z}{dz} \frac{dr}{dz} + V_z \frac{d^2 r}{dz^2} - V_z \frac{dr}{dz} \frac{\partial}{\partial r} \left(\frac{dr}{dz} \right)}{1 + \left(\frac{dr}{dz} \right)^2} \approx \frac{dV_z}{dz} \frac{dr}{dz} + V_z \frac{d^2 r}{dz^2} \quad (C1)$$

This equation applies along streamlines between blade rows. Therefore, local viscous forces may be considered negligible (ref. 7). The assumption was made that the change in flow angle with respect to axial direction along a streamline between blade rows is negligible. Consequently, a combination of continuity, momentum, and Mach number expression yields

$$\frac{dV_z}{dz} = - \frac{V_z}{A(1 - M^2)} \frac{dA}{dz} \quad (C2)$$

After substituting equation (C2) into (C1) the integral equation may be expressed as

$$\int_{r_u}^{r_k} \frac{\partial V_z}{V_z} = - \int_{r_u}^{r_k} \frac{1}{A(1 - M^2)} \frac{dr}{dz} \frac{dA}{dz} \partial r + \int_{r_u}^{r_k} \frac{d^2 r}{dz^2} \partial r \quad (C3)$$

Integration of this expression may be accomplished by a method of finite differences. The substitutions may be clarified by referring to figure 6. The reference stream tube is that extending from r_u to r_k . In the approximation it was assumed that all functions and first and

4238

second derivatives were linear between the two boundaries of the stream tube. This evidently becomes more accurate as $r_k - r_u$ approaches zero. With this assumption the following substitutions can be made:

$$(1) \partial V_z = V_{z,k} - V_{z,u}$$

$$(2) \partial r = r_k - r_u$$

$$(3) V_z = \frac{V_{z,k} + V_{z,u}}{2}$$

$$(4) \frac{dr}{dz} = \frac{\left(\frac{dr}{dz}\right)_k + \left(\frac{dr}{dz}\right)_u}{2}$$

$$(5) \frac{d^2r}{dz^2} = \frac{\left(\frac{d^2r}{dz^2}\right)_k + \left(\frac{d^2r}{dz^2}\right)_u}{2}$$

$$(6) M = \frac{M_k + M_u}{2}$$

(7) $A = \frac{A_k + A_u}{2}$ = Average of areas of stream tubes straddling r_k and r_u , respectively, and from the linearity assumption,

$$A = \pi r_u^2 \left[\left(\frac{r_k}{r_u}\right)^2 - 1 \right]$$

(8) From assumption (7),

$$\frac{dA}{dz} = 2\pi \left[r_k \left(\frac{dr}{dz}\right)_k - r_u \left(\frac{dr}{dz}\right)_u \right] = 2\pi r_u \left[\left(\frac{r_k}{r_u}\right) \left(\frac{dr}{dz}\right)_k - \left(\frac{dr}{dz}\right)_u \right]$$

Making these substitutions into equation (C3) gives

$$\frac{2(V_{z,k} - V_{z,u})}{V_{z,k} + V_{z,u}} = \left\{ \frac{\left[\left(\frac{dr}{dz} \right)_k + \left(\frac{dr}{dz} \right)_u \right] \left[\left(\frac{dr}{dz} \right)_u - \left(\frac{r_k}{r_u} \right) \left(\frac{dr}{dz} \right)_k \right] + \frac{\left(\frac{d^2r}{dz^2} \right)_k + \left(\frac{d^2r}{dz^2} \right)_u}{2}}{r_u \left[\left(\frac{r_k}{r_u} \right)^2 - 1 \right] \left[1 - \left(\frac{M_k + M_u}{2} \right)^2 \right]} \right\} (r_k - r_u) \quad (C4)$$

Since

$$\ln \frac{V_{z,k}}{V_{z,u}} = 2 \left[\frac{(V_{z,k} - V_{z,u})}{(V_{z,k} + V_{z,u})} + \frac{1}{3} \left(\frac{V_{z,k} - V_{z,u}}{V_{z,k} + V_{z,u}} \right)^3 + \frac{1}{5} \left(\frac{V_{z,k} - V_{z,u}}{V_{z,k} + V_{z,u}} \right)^5 + \dots \right]$$

as $r_k - r_u \rightarrow 0$, $V_{z,k} - V_{z,u} \rightarrow 0$, equation (C4) may be rewritten as

$$\ln \frac{V_{z,k}}{V_{z,u}} = \left\{ \frac{\left[\left(\frac{dr}{dz} \right)_k + \left(\frac{dr}{dz} \right)_u \right] \left[\left(\frac{dr}{dz} \right)_u - \left(\frac{r_k}{r_u} \right) \left(\frac{dr}{dz} \right)_k \right] + \frac{\left(\frac{d^2r}{dz^2} \right)_k + \left(\frac{d^2r}{dz^2} \right)_u}{2}}{r_u \left[\left(\frac{r_k}{r_u} \right)^2 - 1 \right] \left[1 - \left(\frac{M_k + M_u}{2} \right)^2 \right]} \right\} (r_k - r_u) \quad (C5)$$

With the assumption of linear variation of the first and second derivatives described in the section "Correction for Radial Flow" the axial velocity ratio for the boundary of the stream tubes, determined from the mass-flow distribution found from the initial design approximation, was calculated.

As an initial assumption in satisfying continuity, the axial velocity on the stream tube boundary nearest the mean radius was taken as the value computed by assuming constant axial velocity after the blade row. The axial velocity at all other radii was found by the solution of equation (C5). The resulting mass flow was integrated and all axial velocities were corrected by the ratio $w_c/w_{\text{integrated}}$ until continuity was satisfied. The boundaries of 10 new stream tubes were then determined by plotting w/w_{total} against radius, where w was the integrated weight flow from the hub to any radius, and corresponding axial velocities were determined by plotting axial velocity against radius and determining the axial velocity at the stream tube boundaries.

REFERENCES

1. Benser, William A.: Analysis of Part-Speed Operation for High-Pressure-Ratio Multistage Axial-Flow Compressors. NACA RM E53L15, 1953.
2. Huppert, Merle C., Calvert, Howard F., and Meyer, André J.: Experimental Investigation of Rotating Stall and Blade Vibration in the Axial-Flow Compressor of a Turbojet Engine. NACA RM E54A08, 1954.
3. Huppert, Merle C., Costilow, Eleanor L., and Budinger, Ray E.: Investigation of a 10-Stage Subsonic Axial-Flow Research Compressor. III - Investigation of Rotating Stall, Blade Vibration, and Surge at Low and Intermediate Compressor Speeds. NACA RM E53C19, 1953.
4. Sandercock, Donald M., Kovach, Karl, and Lieblein, Seymour: Experimental Investigation of a Five-Stage Axial-Flow Research Compressor with Transonic Rotors in All Stages. I - Compressor Design. NACA RM E54F24, 1954.
5. Dugan, James F., Jr.: Effect of Design Over-All Compressor Pressure Ratio Division on Two-Spool Turbojet-Engine Performance and Geometry. NACA RM E54F24a, 1954.
6. Lieblein, Seymour, Schwenk, Francis C., and Broderick, Robert L.: Diffusion Factor for Estimating Losses and Limiting Blade Loadings in Axial-Flow-Compressor Blade Elements. NACA RM E53D01, 1953.
7. Hatch, James E., Giamati, Charles C., and Jackson, Robert J.: Application of Radial-Equilibrium Condition to Axial-Flow Turbomachine Design Including Consideration of Change of Entropy with Radius Downstream of Blade Row. NACA RM E54A20, 1954.
8. Wu, Chung-Hua, and Wolfenstein, Lincoln: Application of Radial-Equilibrium Condition to Axial-Flow Compressor and Turbine Design. NACA Rep. 955, 1950. (Supersedes NACA TN 1795.)
9. Stanitz, John D.: Effect of Blade-Thickness Taper on Axial-Velocity Distribution at the Leading Edge of an Entrance Rotor-Blade Row with Axial Inlet, and the Influence of This Distribution on Alignment of the Rotor Blade for Zero Angle of Attack. NACA TN 2986, 1953.
10. Klapproth, John F.: General Considerations of Mach Number Effects on Compressor-Blade Design. NACA RM E53L23a, 1954.
11. Robbins, William H., Jackson, Robert J., and Lieblein, Seymour: Blade-Element Flow in Annular Cascades. Ch. VII of Aerodynamic Design of Axial-Flow Compressors, vol. II. NACA RM E56B03a, 1956.

12. Graham, Robert W., and Costilow, Eleanor L.: Compressor Stall and Blade Vibration. Ch. XI of Aerodynamic Design of Axial-Flow Compressors, vol. III. NACA RM E56B03b, 1956.
13. Wright, Linwood C., and Wilcox, Ward W.: Investigation of Two-Stage Counterrotating Compressor. II - First-Rotor Blade-Element Performance. NACA RM E56G09, 1956.
14. Fessler, Theodore E., and Hartmann, Melvin J.: Preliminary Survey of Compressor Rotor-Blade Wakes and Other Flow Phenomena with a Hot-Wire Anemometer. NACA RM E56A13, 1956.
15. Staniforth, R.: A Note on Compressor Operation at Transonic Relative Inlet Mach Numbers. Memo. M.224, British N.G.T.E., July 1954.
16. The Staff of the Ames 1- by 3-Foot Supersonic Wind-Tunnel Section: Notes and Tables for Use in the Analysis of Supersonic Flow. NACA TN 1428, 1947.
17. Keenan, Joseph H., and Kaye, Joseph: Gas Tables, Thermodynamic Properties of Air. John Wiley & Sons, Inc., 1948.

TABLE I. - TOTAL-PRESSURE AND TOTAL-TEMPERATURE
VARIATIONS WITH AXIAL AND RADIAL STATIONS
FOR STANDARD SEA-LEVEL INLET CONDITIONS

| Axial position | Radial position | Total pressure, lb/sq ft | Total temperature, °R |
|---------------------|-----------------|--------------------------|-----------------------|
| Inlet | Tip | 2116 | 518.7 |
| | Mean | ↓ | ↓ |
| | Hub | ↓ | ↓ |
| After first rotor | Tip | 2960 | 575.8 |
| | Mean | ↓ | ↓ |
| | Hub | ↓ | ↓ |
| After first stator | Tip | 2950 | 575.8 |
| | Mean | 2949 | ↓ |
| | Hub | 2947 | ↓ |
| After second rotor | Tip | 4304 | 648.6 |
| | Mean | 4303 | ↓ |
| | Hub | 4300 | ↓ |
| After second stator | Tip | 4290 | 648.6 |
| | Mean | 4287 | ↓ |
| | Hub | 4282 | ↓ |
| After struts | Tip | 4283 | 648.6 |
| | Mean | 4280 | ↓ |
| | Hub | 4275 | ↓ |

TABLE II. - NUMBER OF BLADES, CHORD LENGTH, AND
SOLIDITY IN EACH BLADE ROW

| Blade row | Radial position | Number of blades | Chord, in. | Solidity |
|---------------|-----------------|------------------|------------|----------|
| First rotor | Tip | 37 | 2.018 | 1.008 |
| | Mean | | ↓ | 1.433 |
| | Hub | | ↓ | 2.478 |
| First stator | Tip | 38 | 1.945 | 1.000 |
| | Mean | | ↓ | 1.327 |
| | Hub | | ↓ | 1.970 |
| Second rotor | Tip | 41 | 2.100 | 1.165 |
| | Mean | | ↓ | 1.475 |
| | Hub | | ↓ | 2.008 |
| Second stator | Tip | 40 | 1.848 | 1.000 |
| | Mean | | ↓ | 1.226 |
| | Hub | | ↓ | 1.584 |

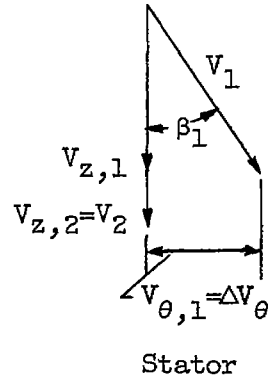
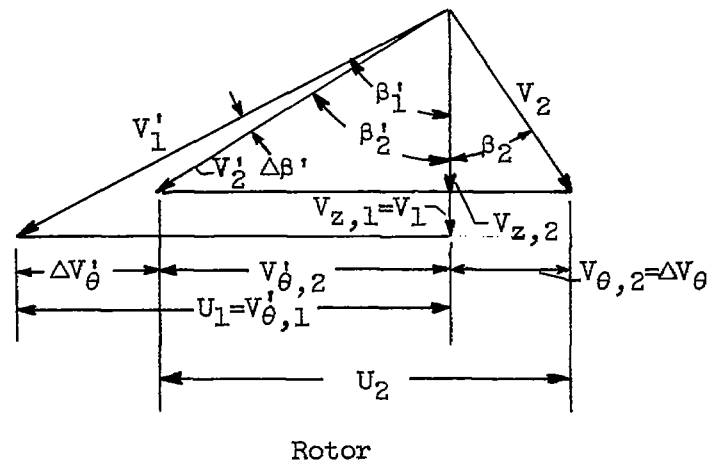


Figure 1. - Typical rotor and stator velocity diagrams.

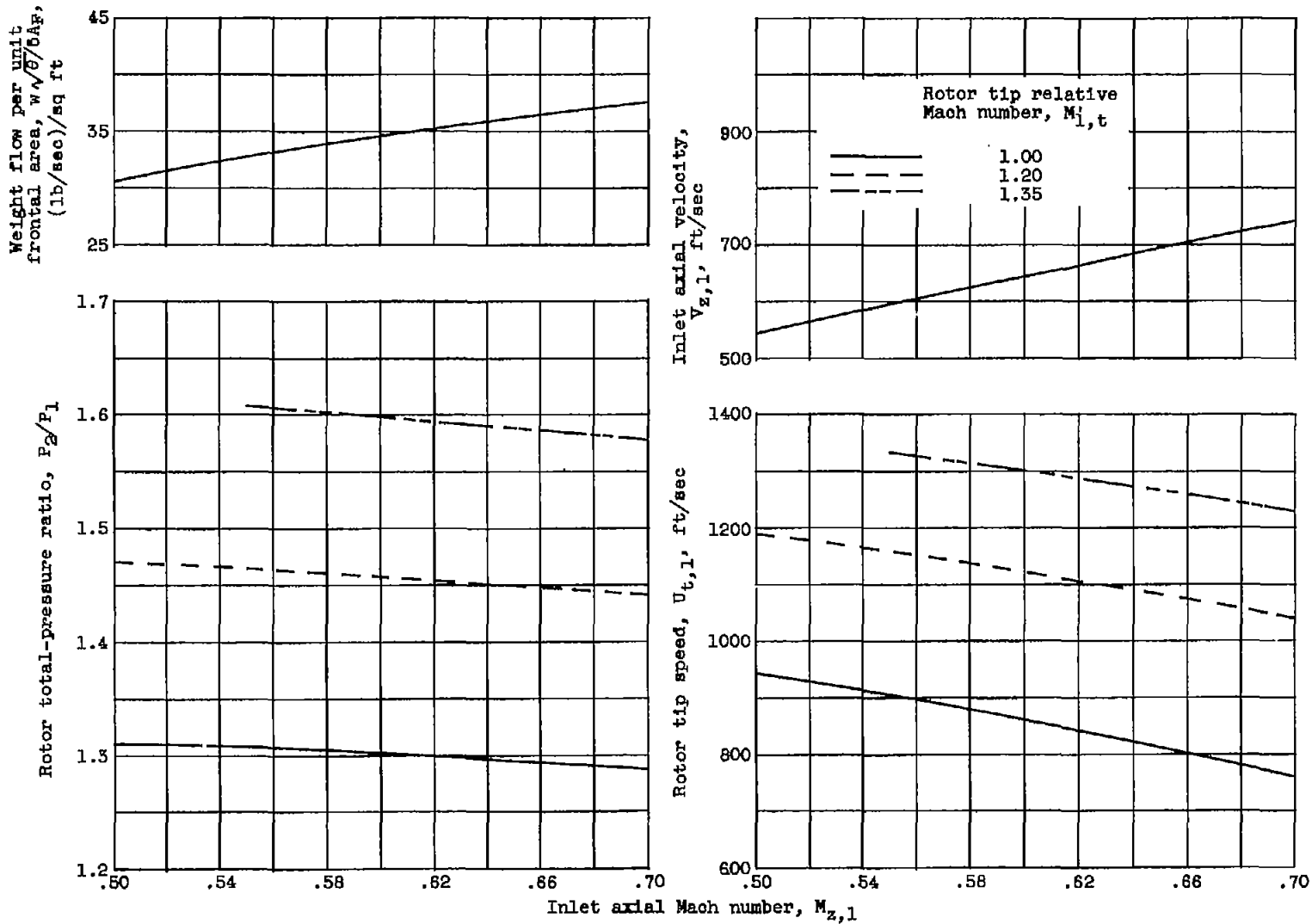
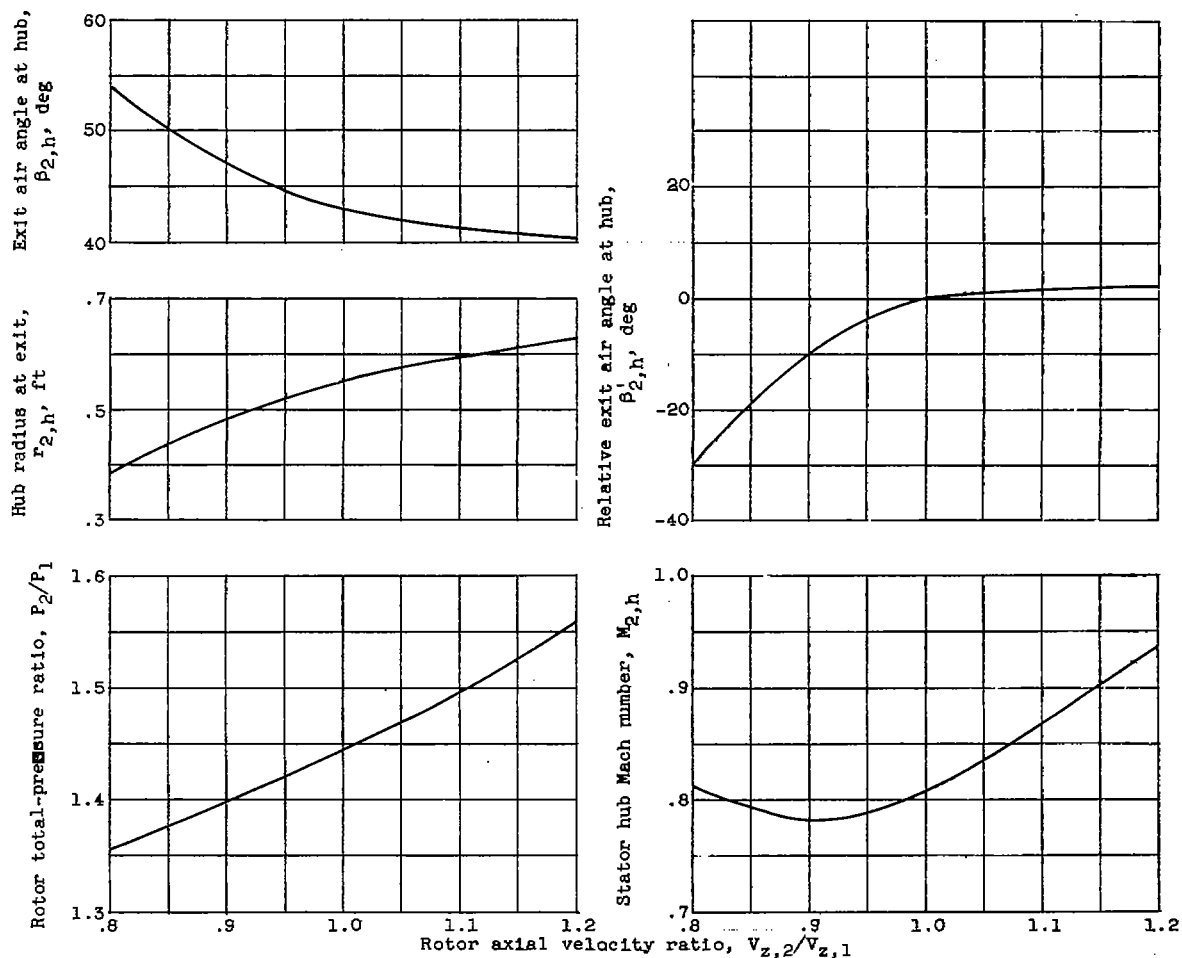
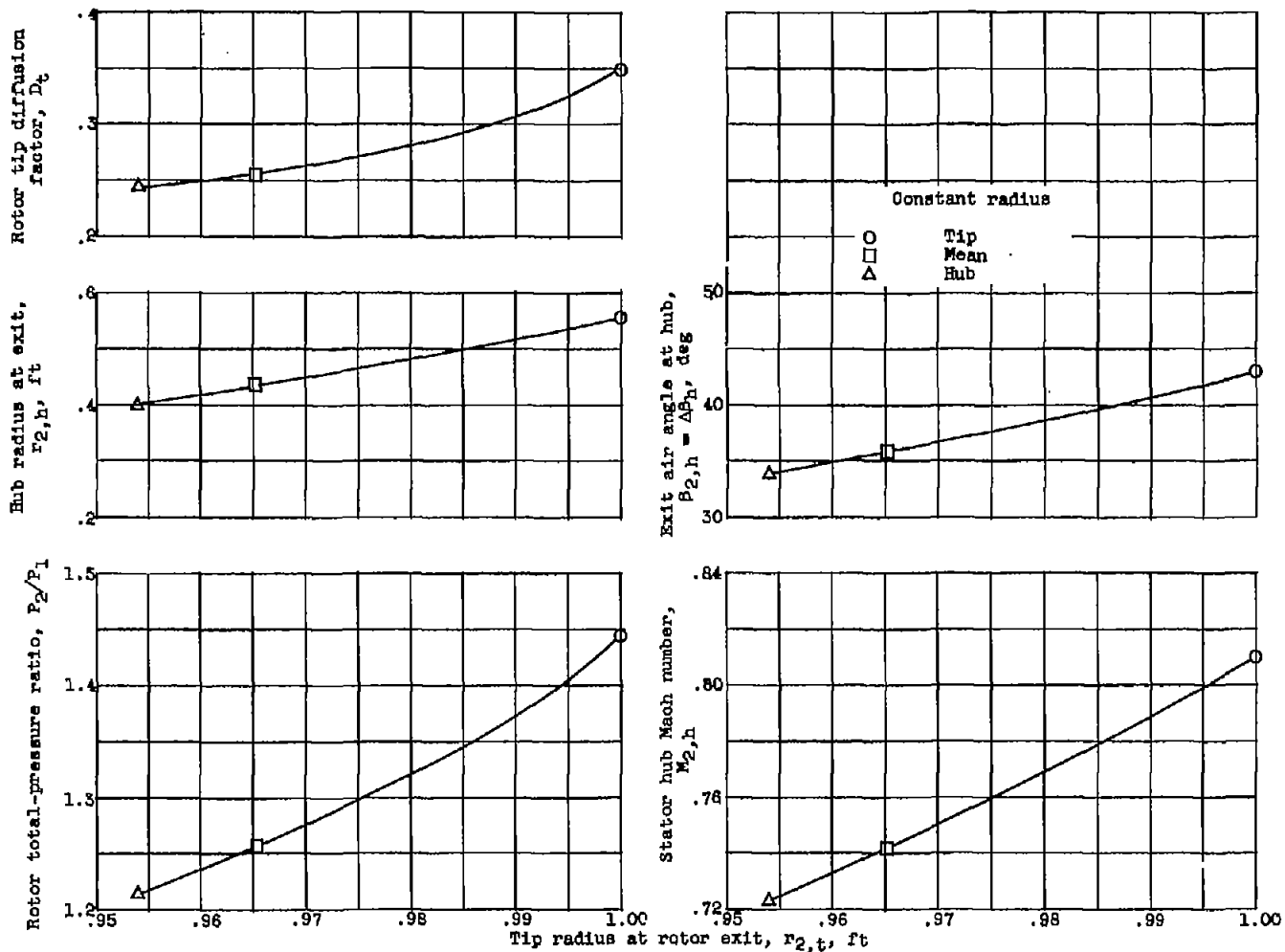


Figure 2. - Effect of inlet relative and axial Mach numbers on first-rotor parameters. Rotor tip diffusion factor, 0.55; axial velocity ratio across first rotor, 1.0; hub radius at inlet, 0.4 foot; tip radius at rotor exit, 1.0 foot; rotor polytropic efficiency, 0.92; boundary-layer-blockage correction, 1 percent.



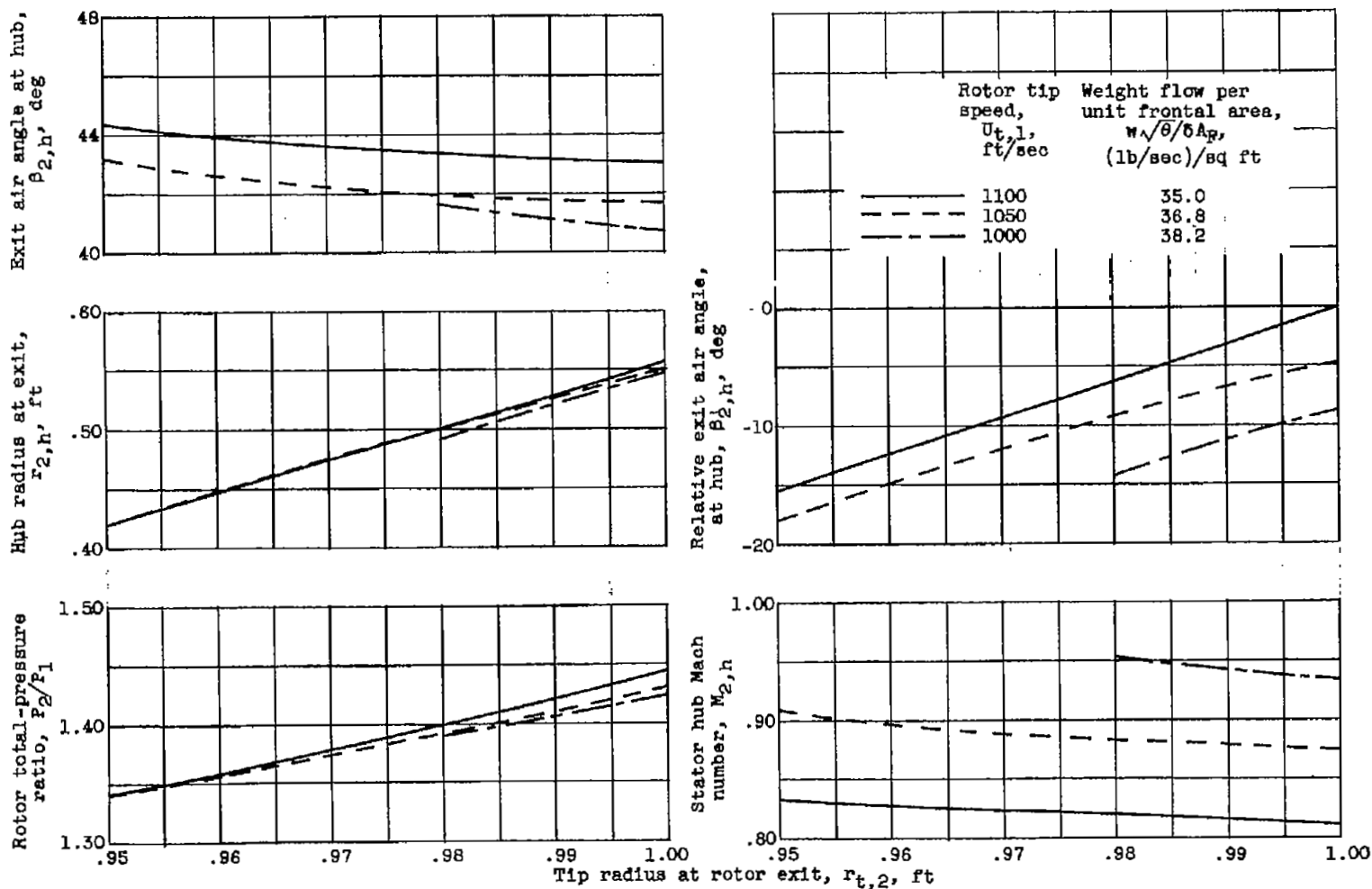
(a) Axial velocity ratio. Tip diffusion factor, 0.35; weight flow per unit frontal area, 35 pounds per second per square foot; rotor tip speed, 1100 feet per second; tip radius at rotor inlet and exit, 1.0 foot.

Figure 3. - Effect of variables on first-stage parameters. Hub radius at rotor inlet, 0.4 foot; boundary-layer-blockage correction at rotor inlet, 1 percent; boundary-layer-blockage correction at rotor exit, 2 percent; rotor polytropic efficiency, 0.92.



(b) Rotor tip exit radius. Rotor tip speed, 1100 feet per second; weight flow per unit frontal area, 35 pounds per second per square foot; tip radius at rotor inlet, 1 foot; axial velocity ratio across first rotor, 1.0; relative exit air angle at rotor hub, 0° .

Figure 3. - Continued. Effect of variables on first-stage parameters. Hub radius at rotor inlet, 0.4 foot; boundary-layer-blockage correction at rotor inlet, 1 percent; boundary-layer-blockage correction at rotor exit, 2 percent; rotor polytropic efficiency, 0.92.



(c) Rotor tip speed and exit radius. Tip diffusion factor, 0.35; tip radius at rotor inlet, 1.0 foot; rotor tip relative Mach number, 1.188; axial velocity ratio across rotor, 1.0.

Figure 3. - Concluded. Effect of variables on first-stage parameters. Hub radius at rotor inlet, 0.4 foot; boundary-layer-blockage correction at rotor inlet, 1 percent; boundary-layer-blockage correction at rotor exit, 2 percent; rotor polytropic efficiency, 0.92.

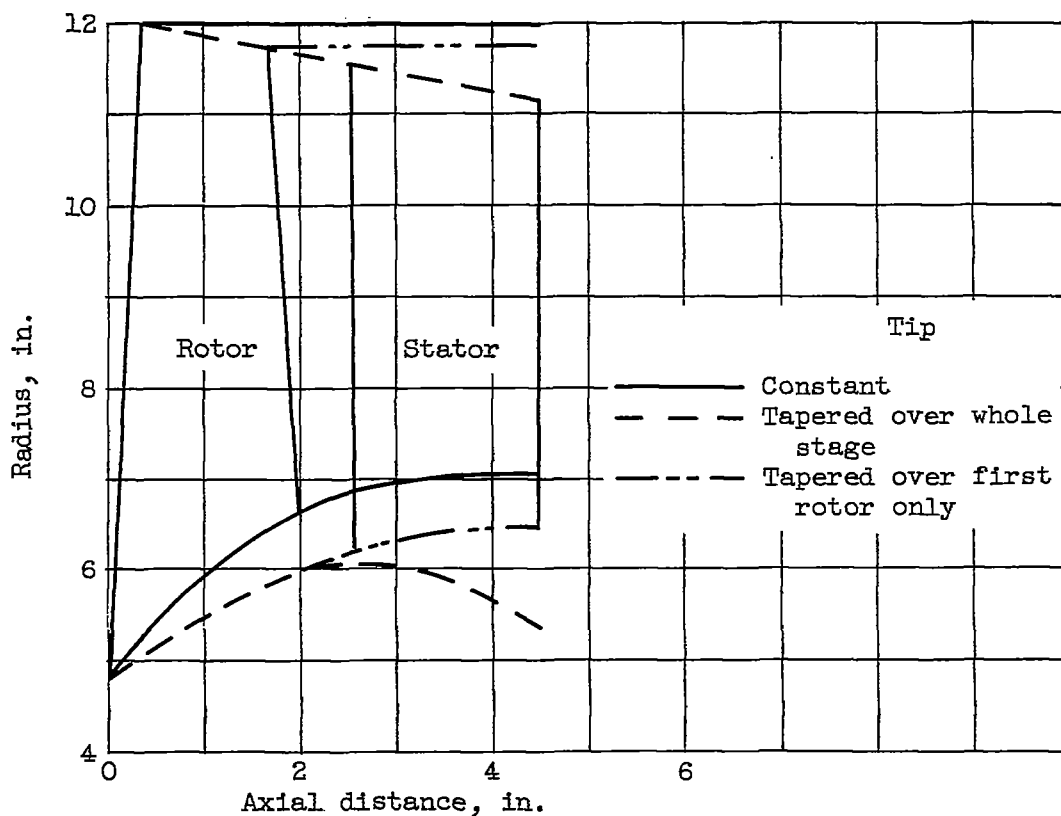


Figure 4. - Effect of tip taper on first-stage hub contour. Axial velocity at inlet to rotor and stator and at exit from stator, 658 feet per second; rotor tip speed, 1100 feet per second; weight flow per unit frontal area, 35 pounds per second per square foot; rotor polytropic efficiency, 0.92; tip diffusion factor, 0.35.

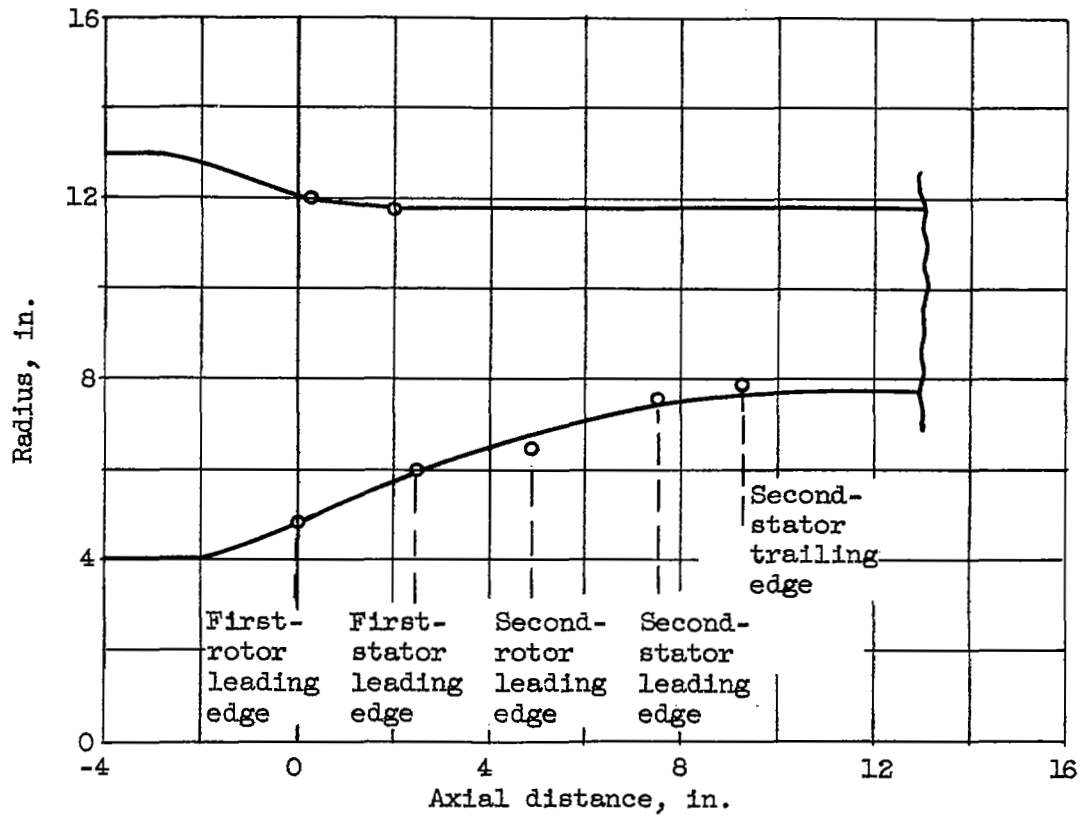


Figure 5. - First-spool passage contour.

4288

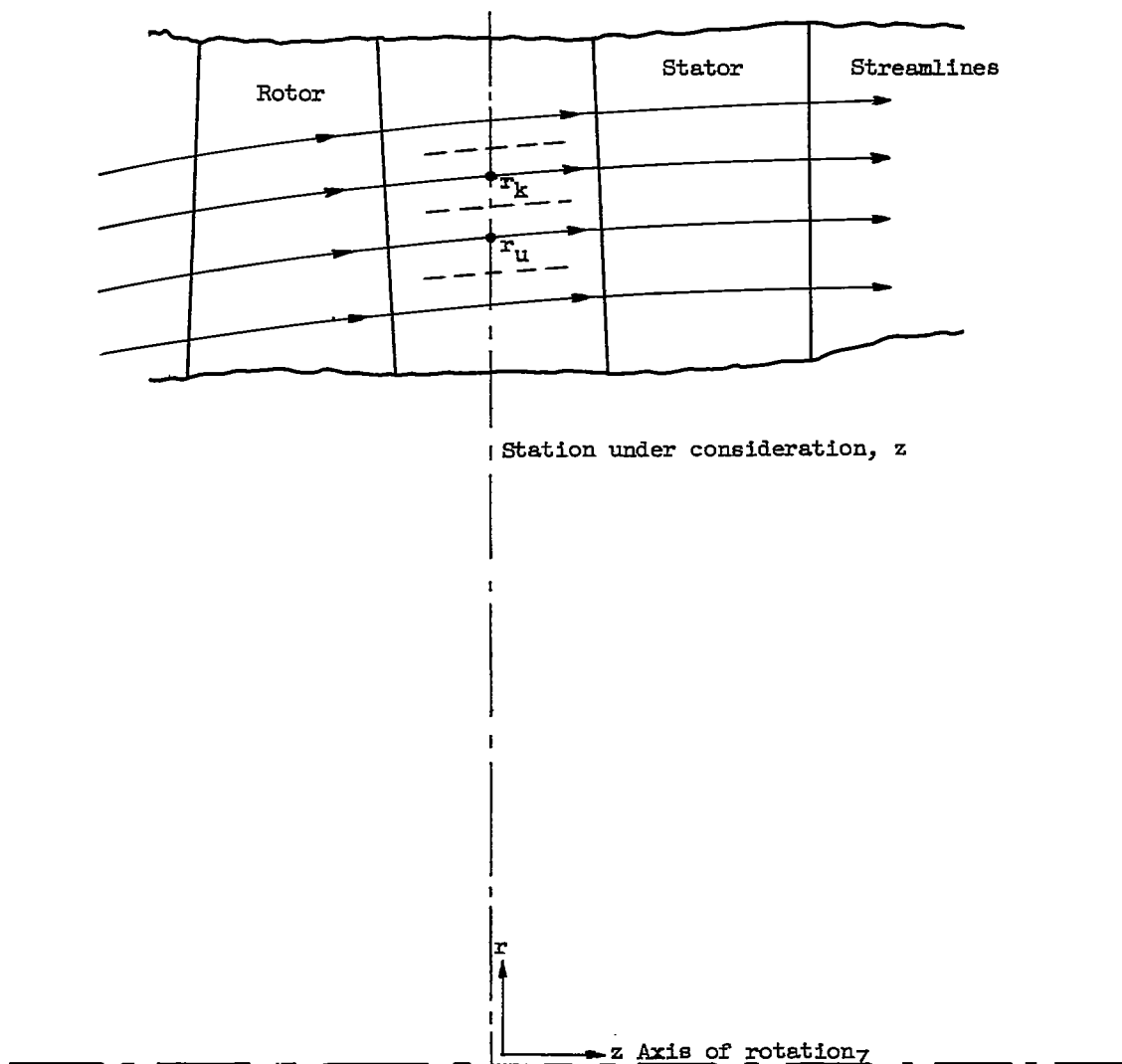
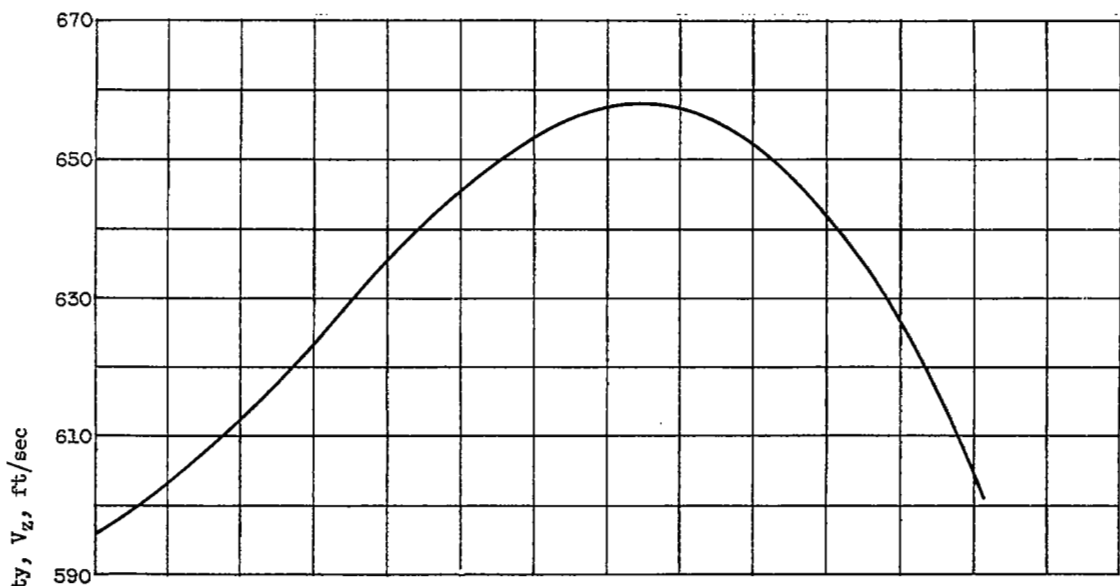
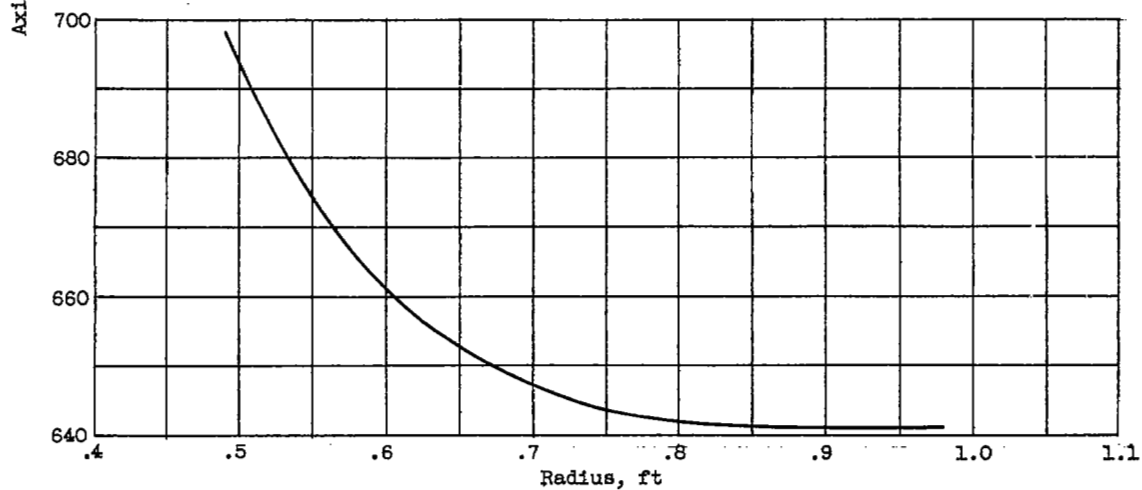


Figure 6. - Sketch of stream tubes on r, z surface.



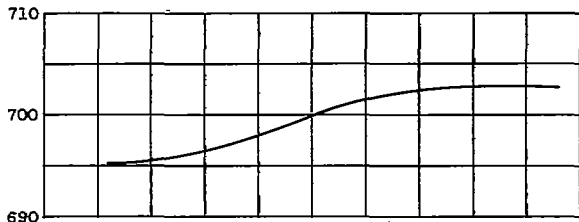
(a) Inlet to compressor. Tip streamline first derivative, -0.32 ; tip streamline second derivative, 0 ; hub streamline first derivative, 0.51 ; hub streamline second derivative, 0 ; axial distance from inlet to first rotor, 0 .



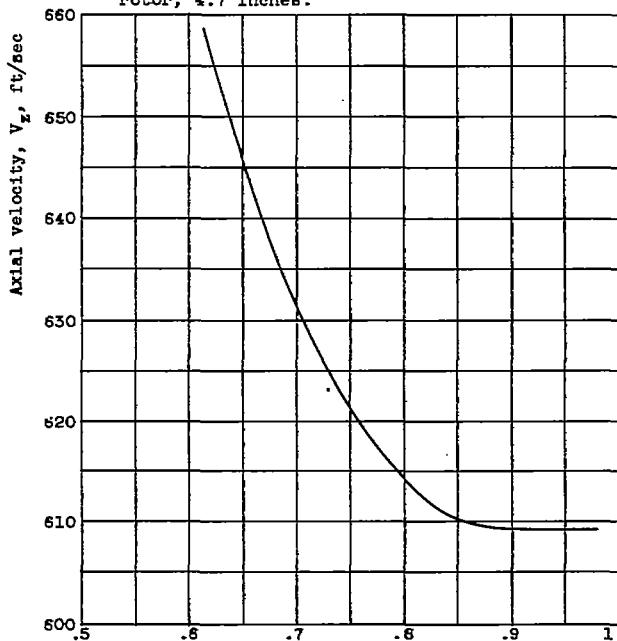
(b) After first rotor. Tip streamline first and second derivatives, 0 ; hub streamline first derivative, 0.443 ; hub streamline second derivative, -1.17 ; axial distance from inlet to first rotor, 2.2 inches.

Figure 7. - Variation of axial velocity with radius.

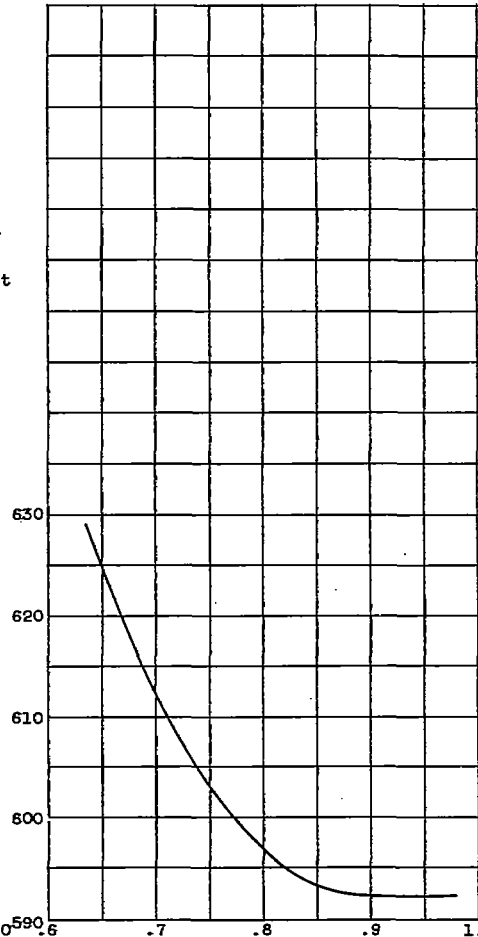
4288



(c) After first stator. Tip streamline first and second derivatives, 0; hub streamline first derivative, 0.273; hub streamline second derivative, -0.19; axial distance from inlet to first rotor, 4.7 inches.



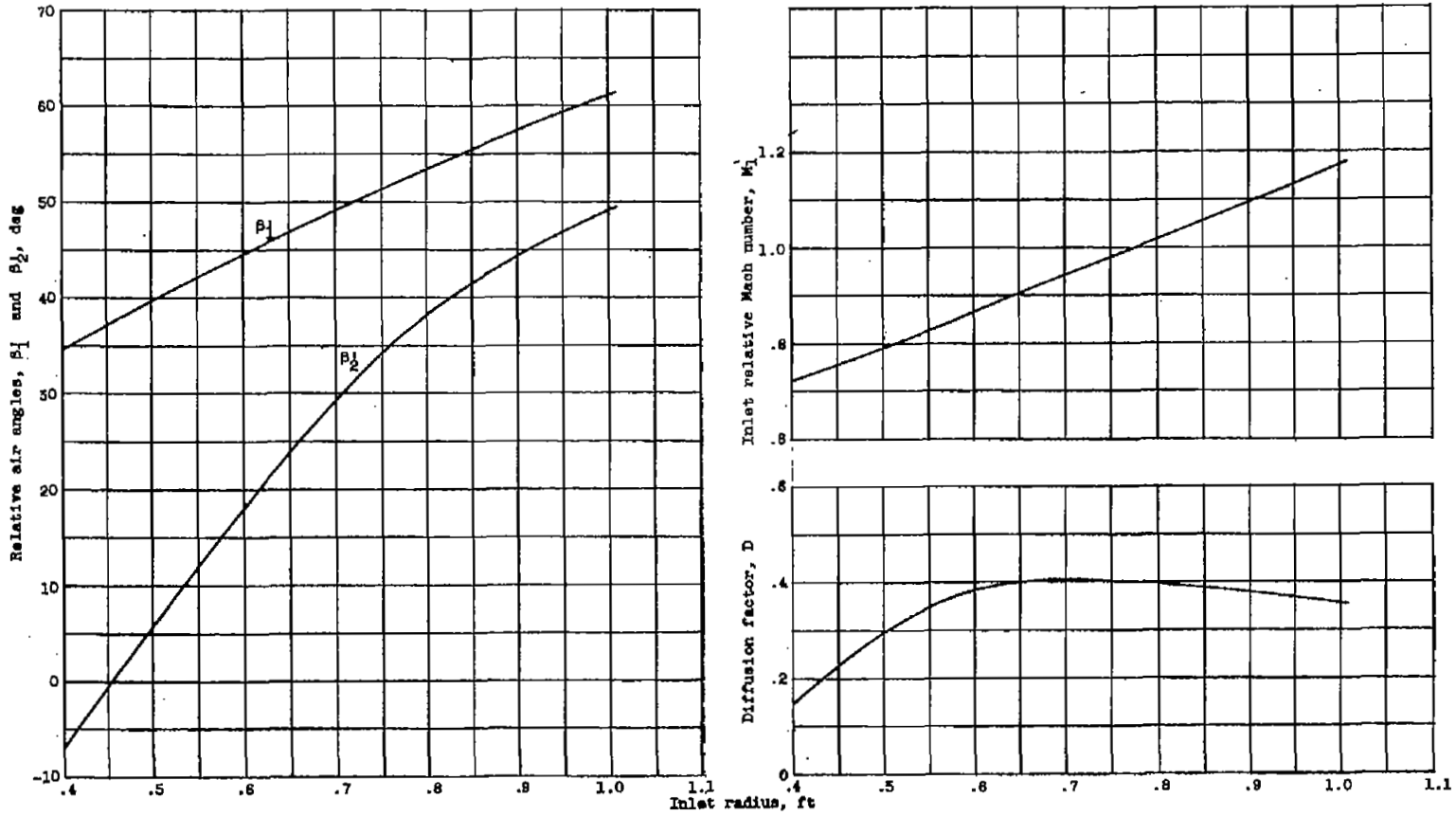
(d) After second rotor. Tip streamline first and second derivatives, 0; hub streamline first derivative, 0.194; hub streamline second derivative, -0.77; axial distance from inlet to first rotor, 7.2 inches.



(e) After second stator. Tip streamline first and second derivatives, 0; hub streamline first derivative, 0.072; hub streamline second derivative, -0.49; axial distance from inlet to first rotor, 9.37 inches.

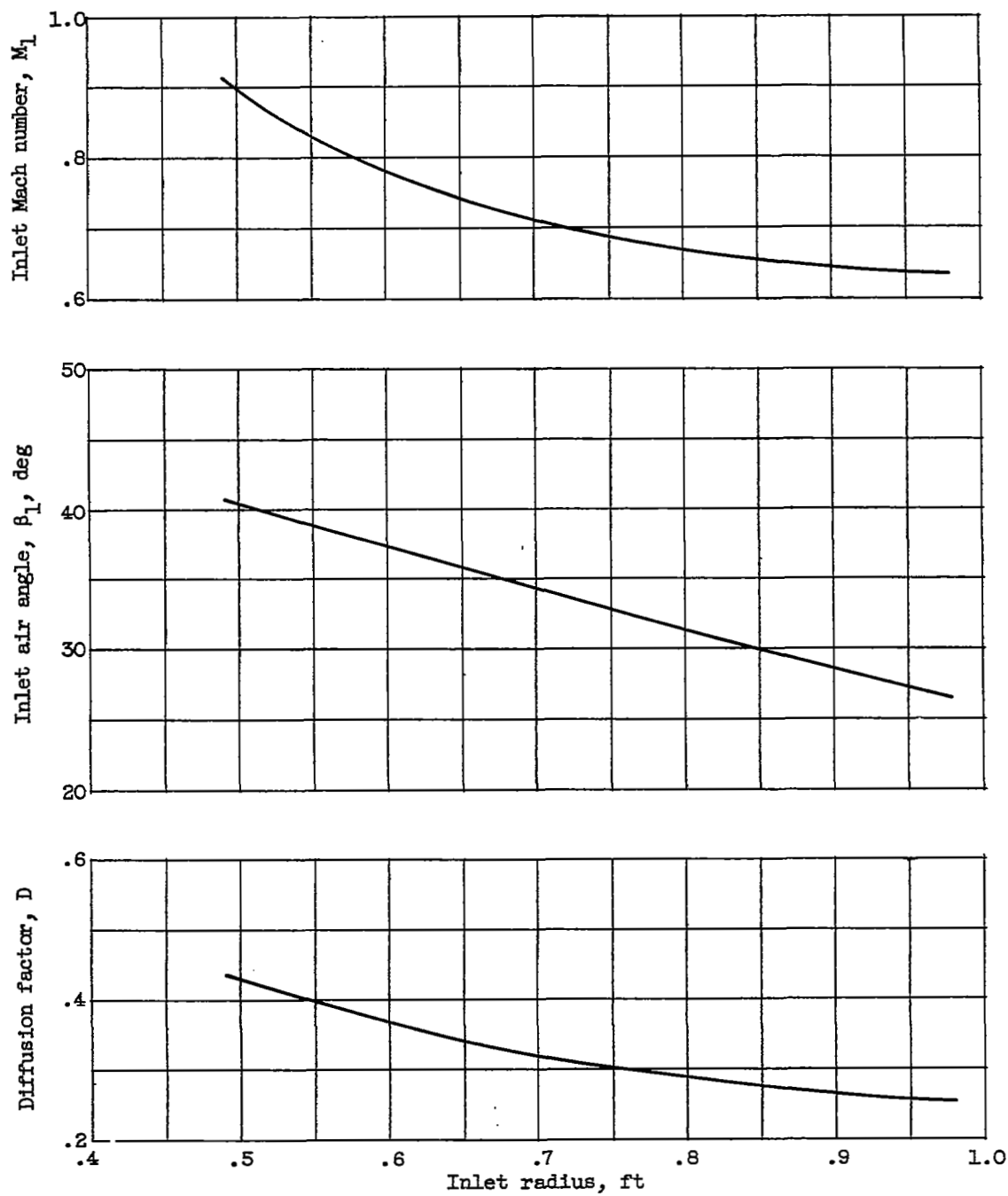
Figure 7. - Concluded. Variation of axial velocity with radius.

CB-6



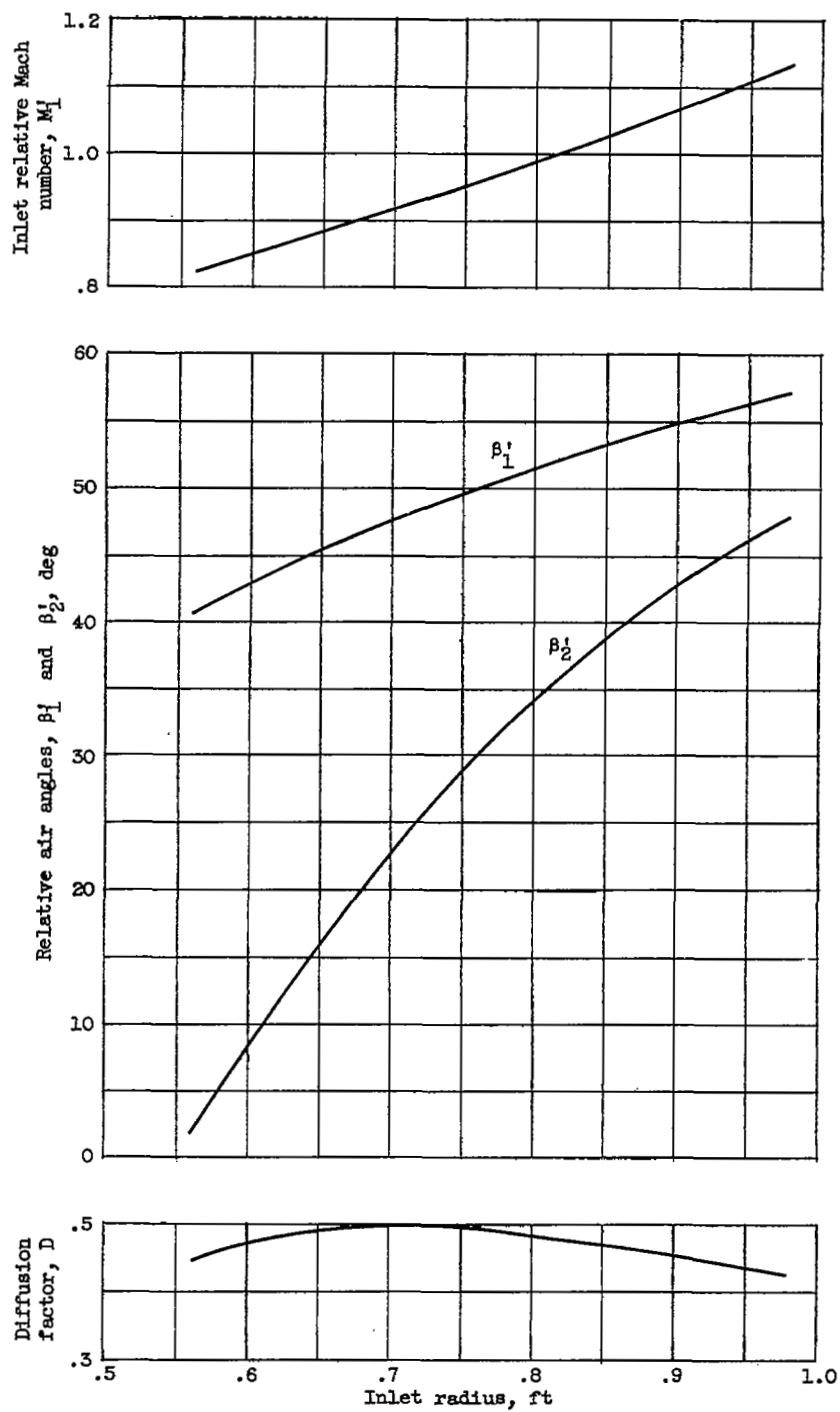
(a) First rotor.

Figure 8. - Variation with radius of air angles, Mach number, and diffusion factor used in final design.



(b) First stator.

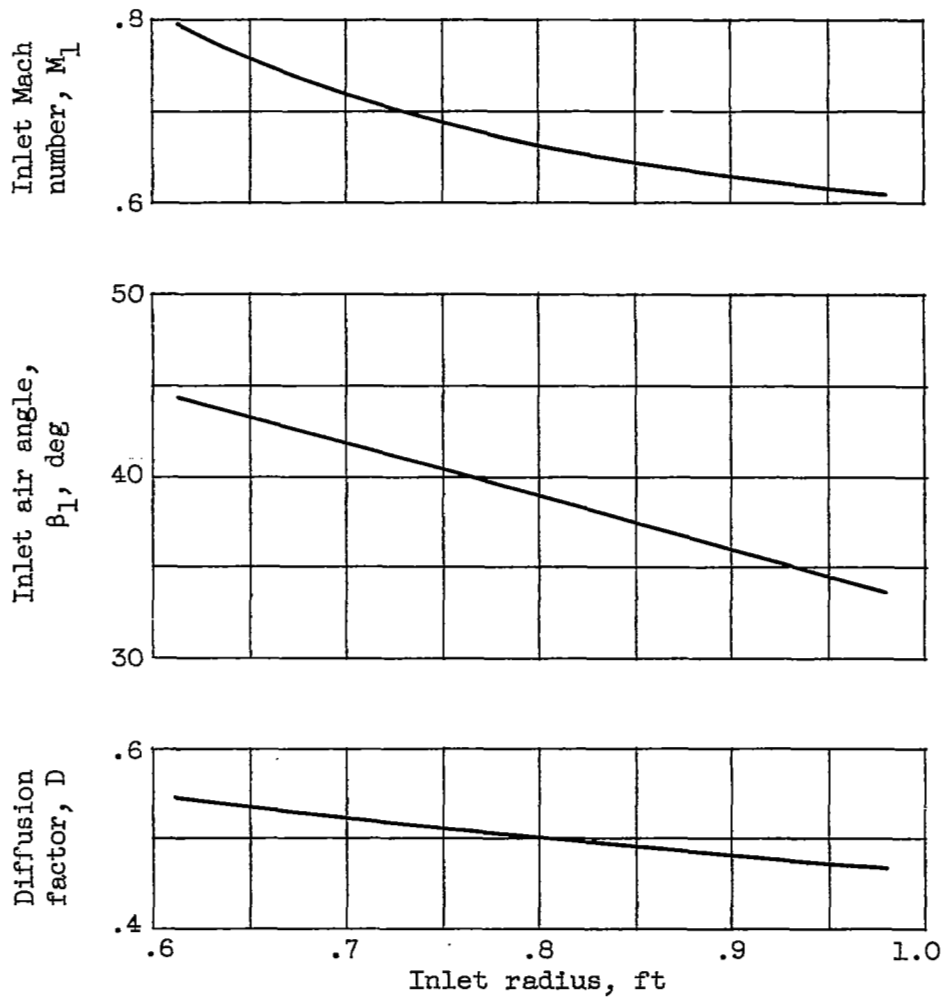
Figure 8. - Continued. Variation with radius of air angles, Mach number, and diffusion factor used in final design.



(c) Second rotor.

Figure 8. - Continued. Variation with radius of air angles, Mach number, and diffusion factor used in final design.

4288



(d) Second stator.

Figure 8. - Concluded. Variation with radius of air angles, Mach number, and diffusion factor used in final design.

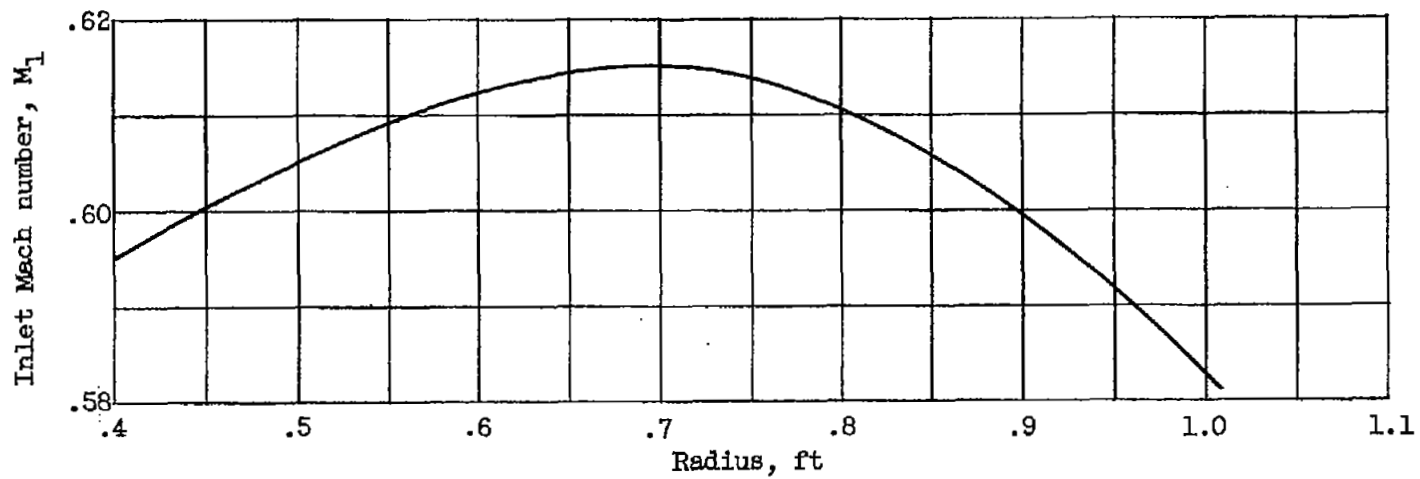


Figure 9. - Mach number distribution at inlet to compressor used in final design.

4288

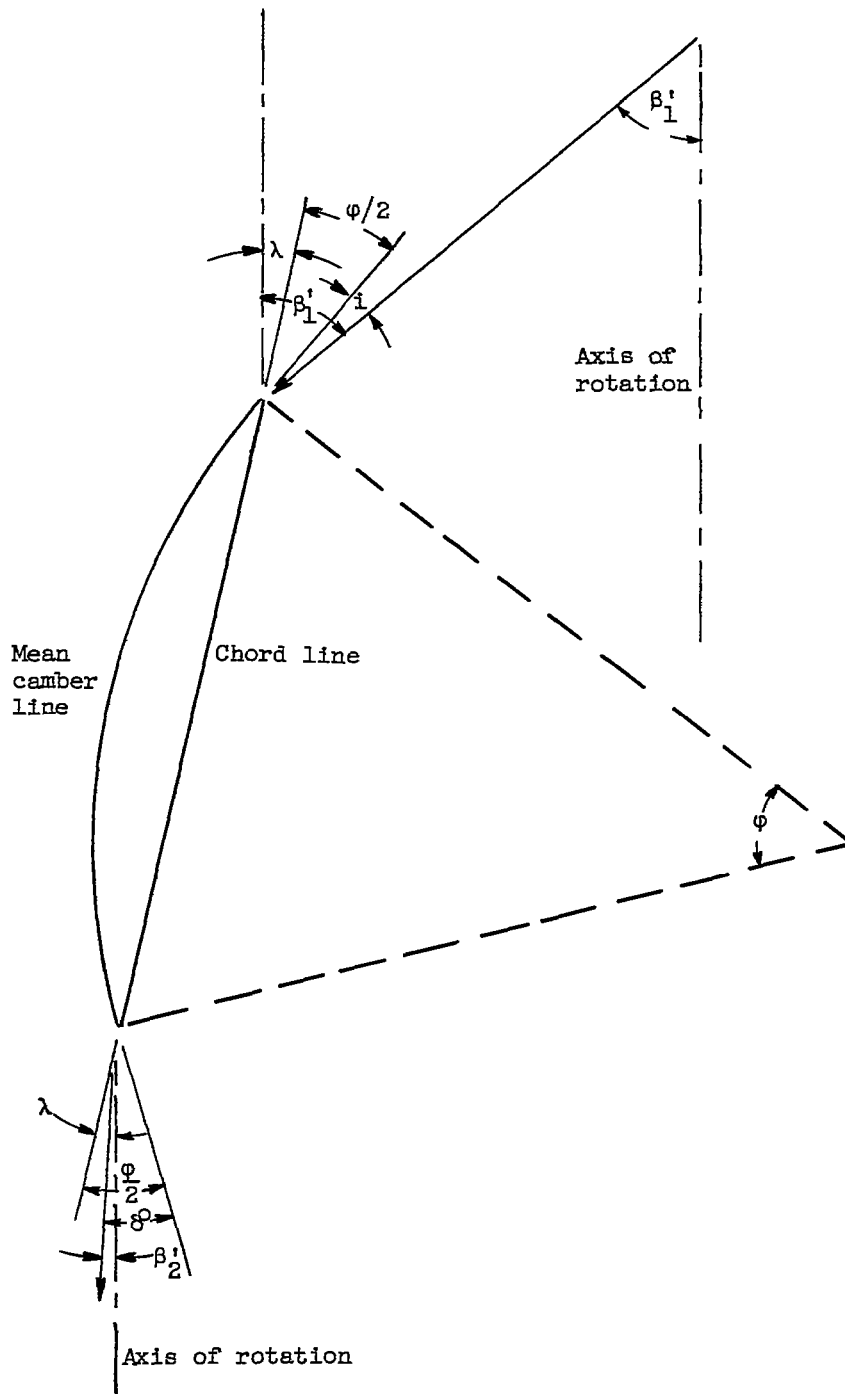


Figure 10. - Angle relations of double-circular-arc element.

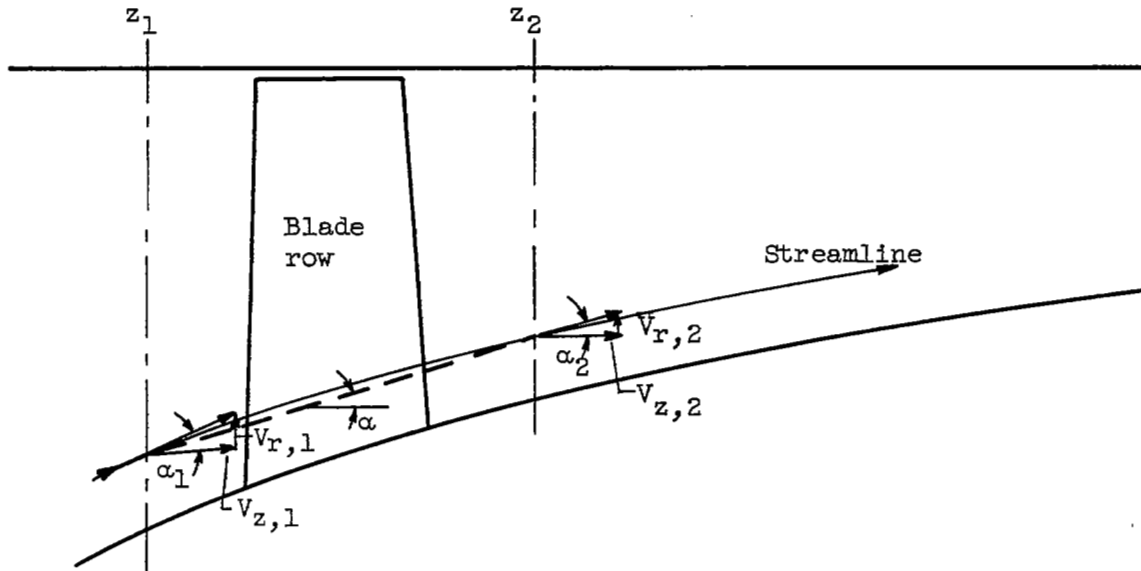
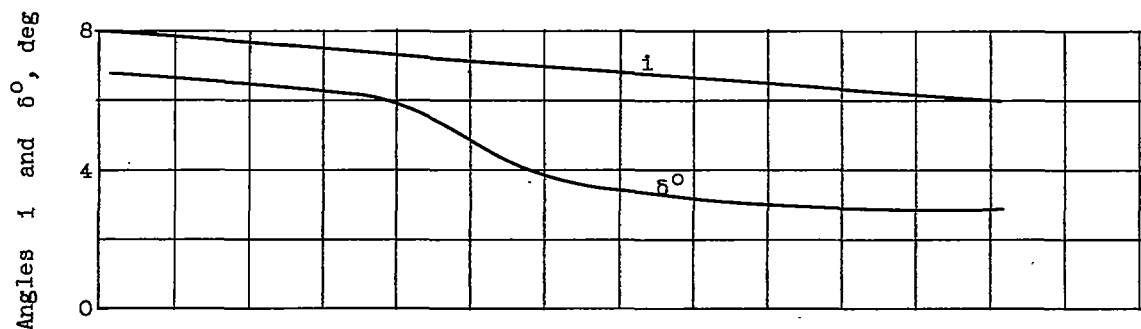
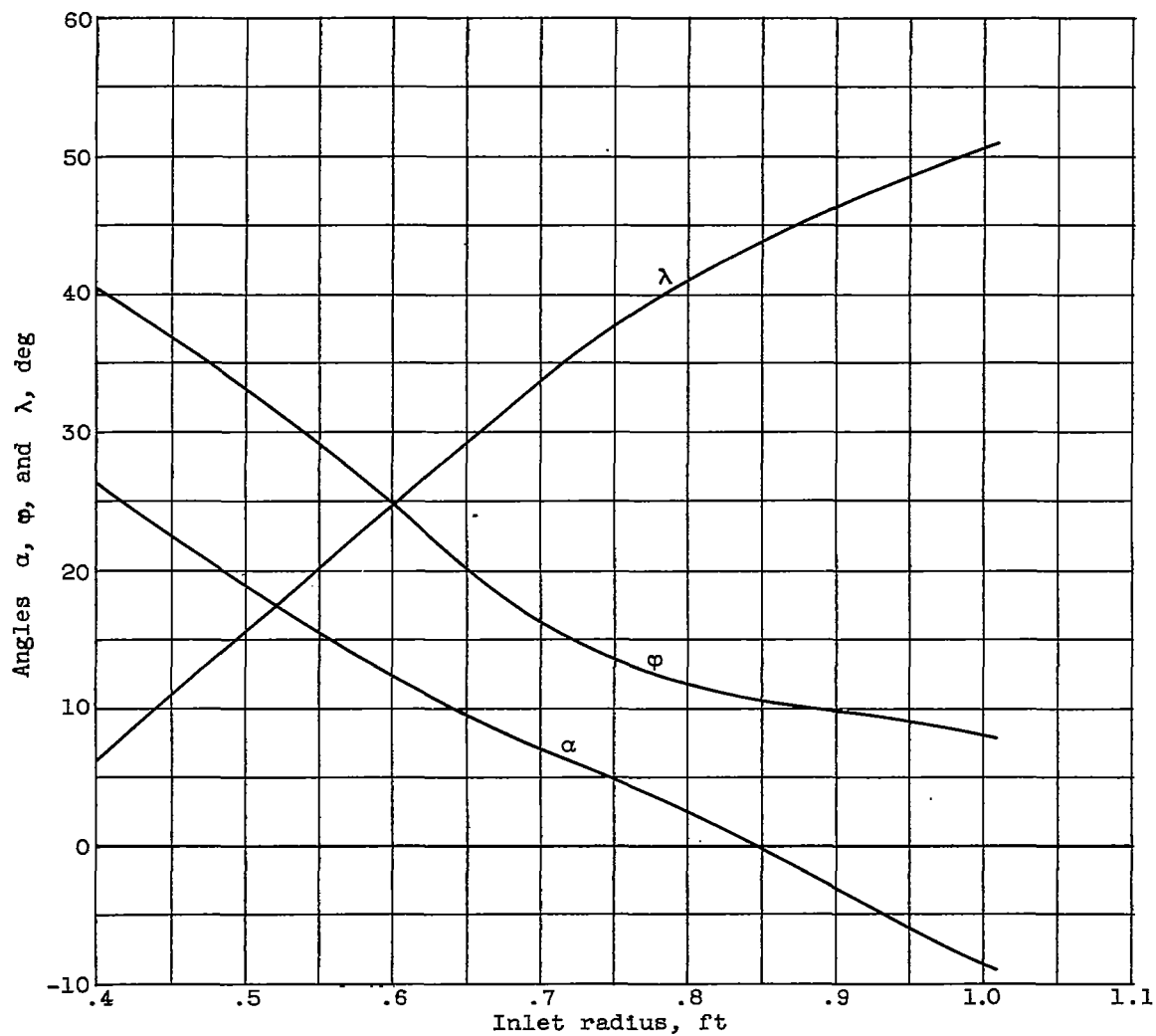


Figure 11. - Sketch of streamline on r, z surface.

4288

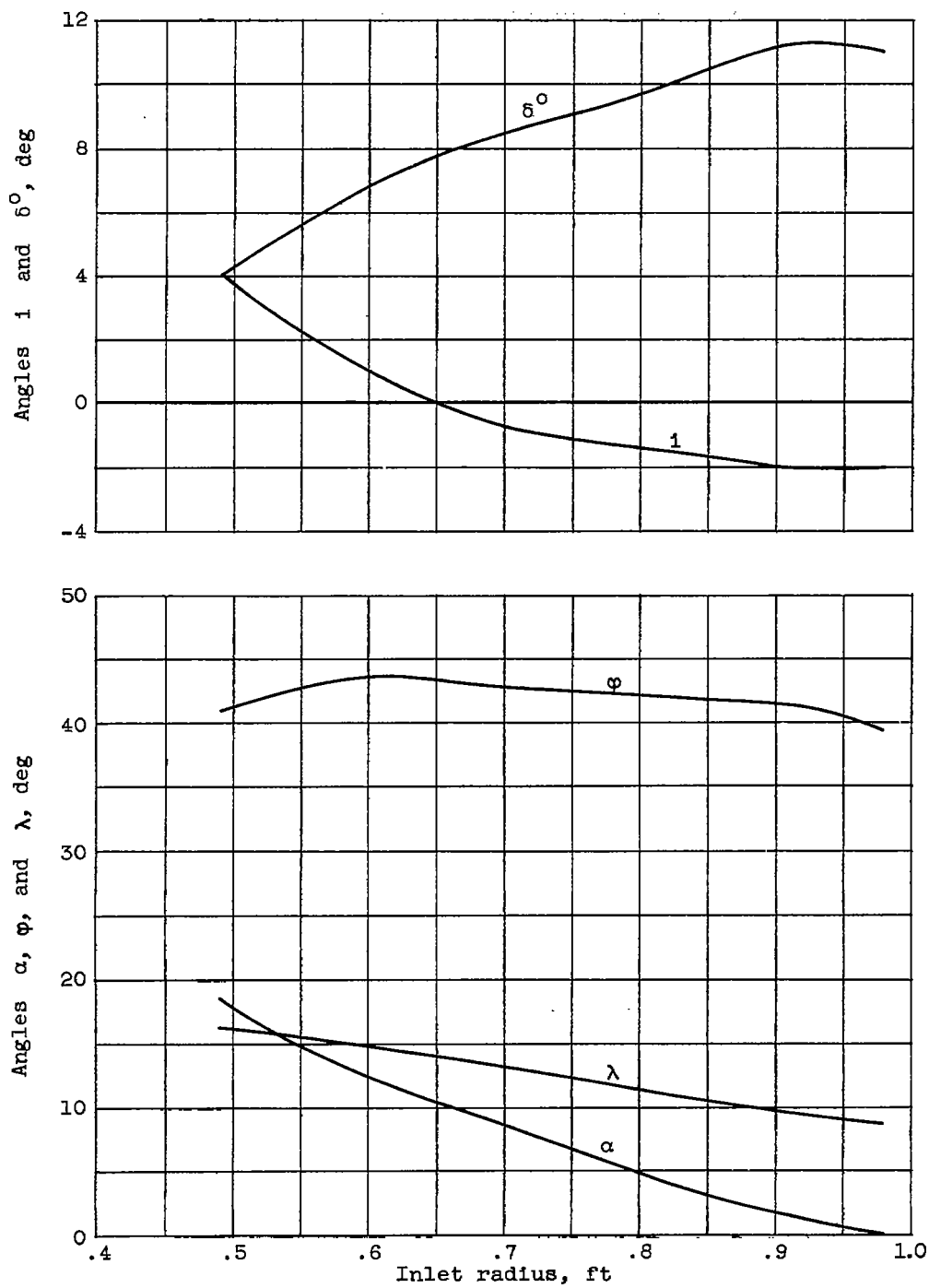


CB-7



(a) First rotor.

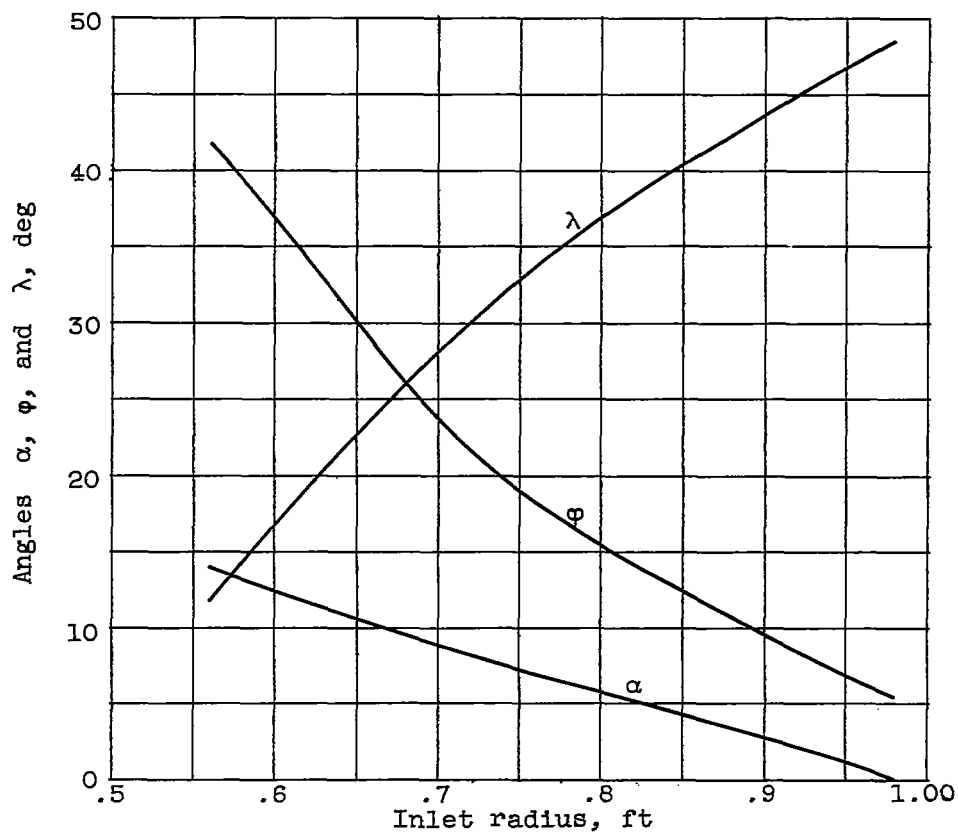
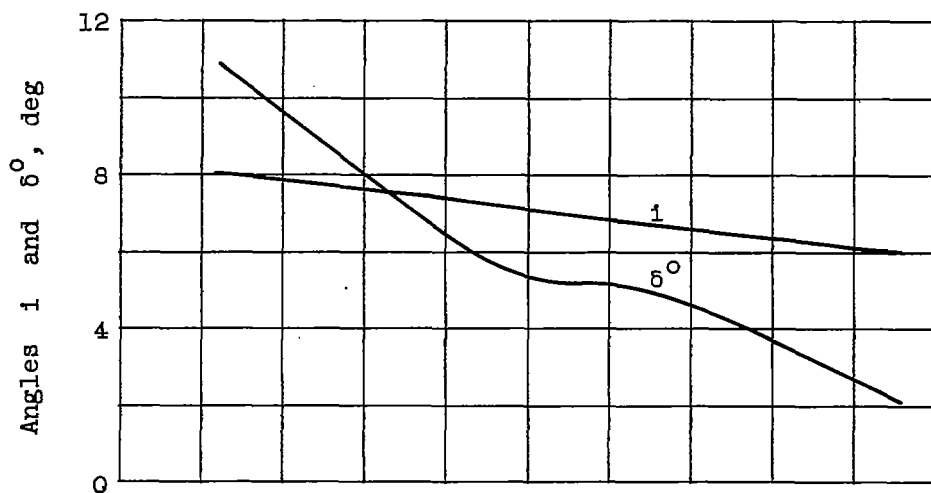
Figure 12. - Stator and rotor blade row airfoil-section characteristics.



(b) First stator.

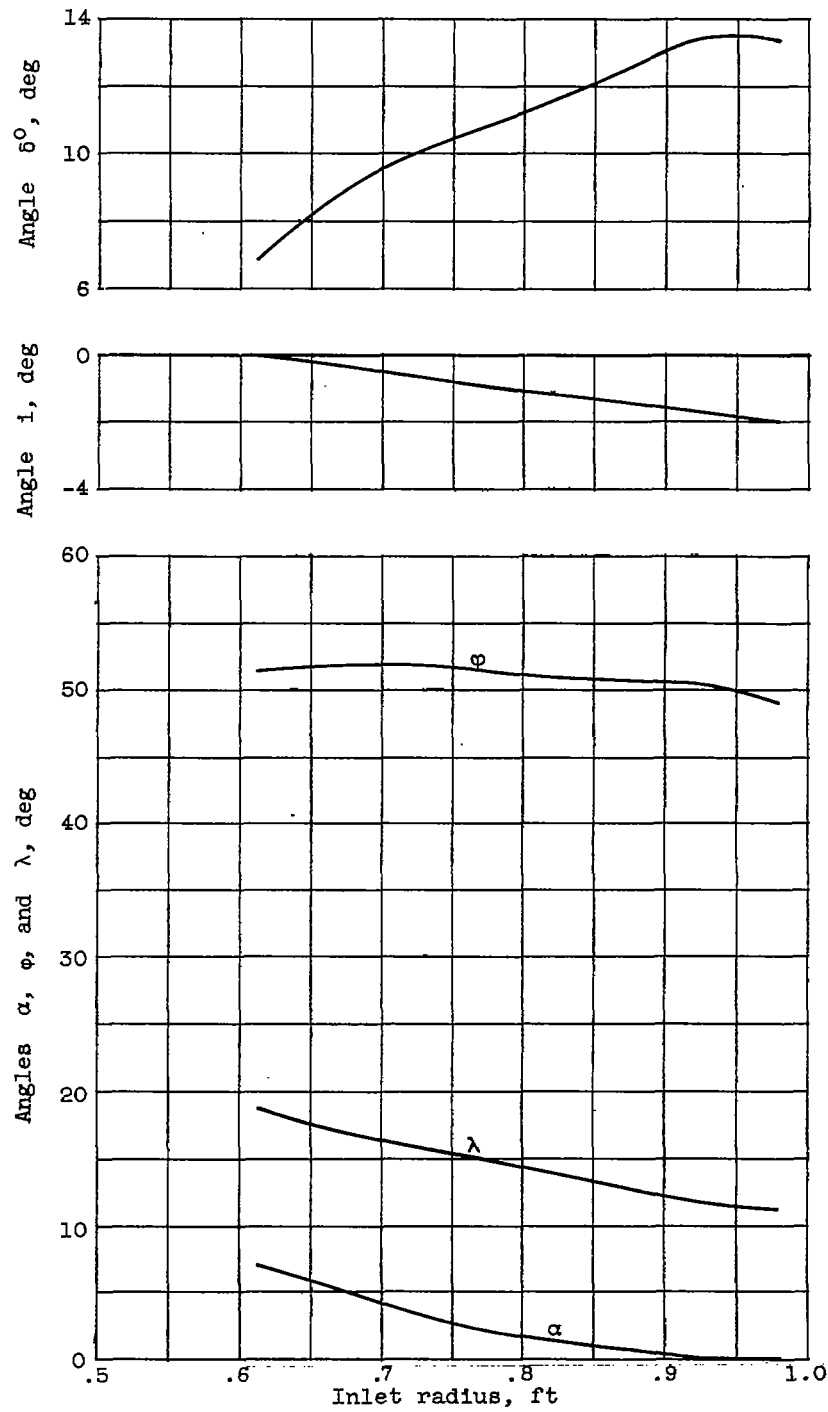
Figure 12. - Continued. Stator and rotor blade row airfoil-section characteristics.

4288



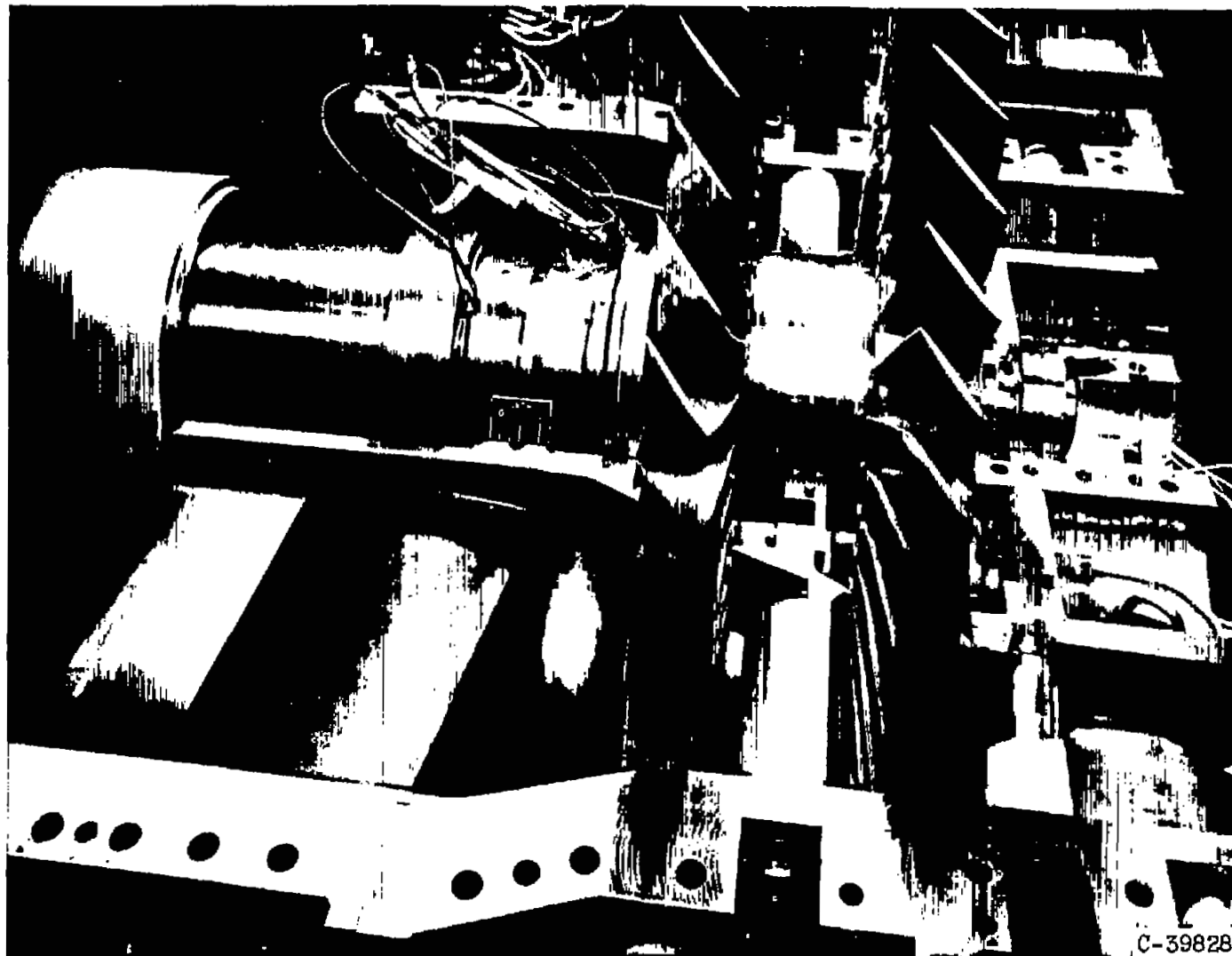
(c) Second rotor.

Figure 12. - Continued. Stator and rotor blade row airfoil-section characteristics.



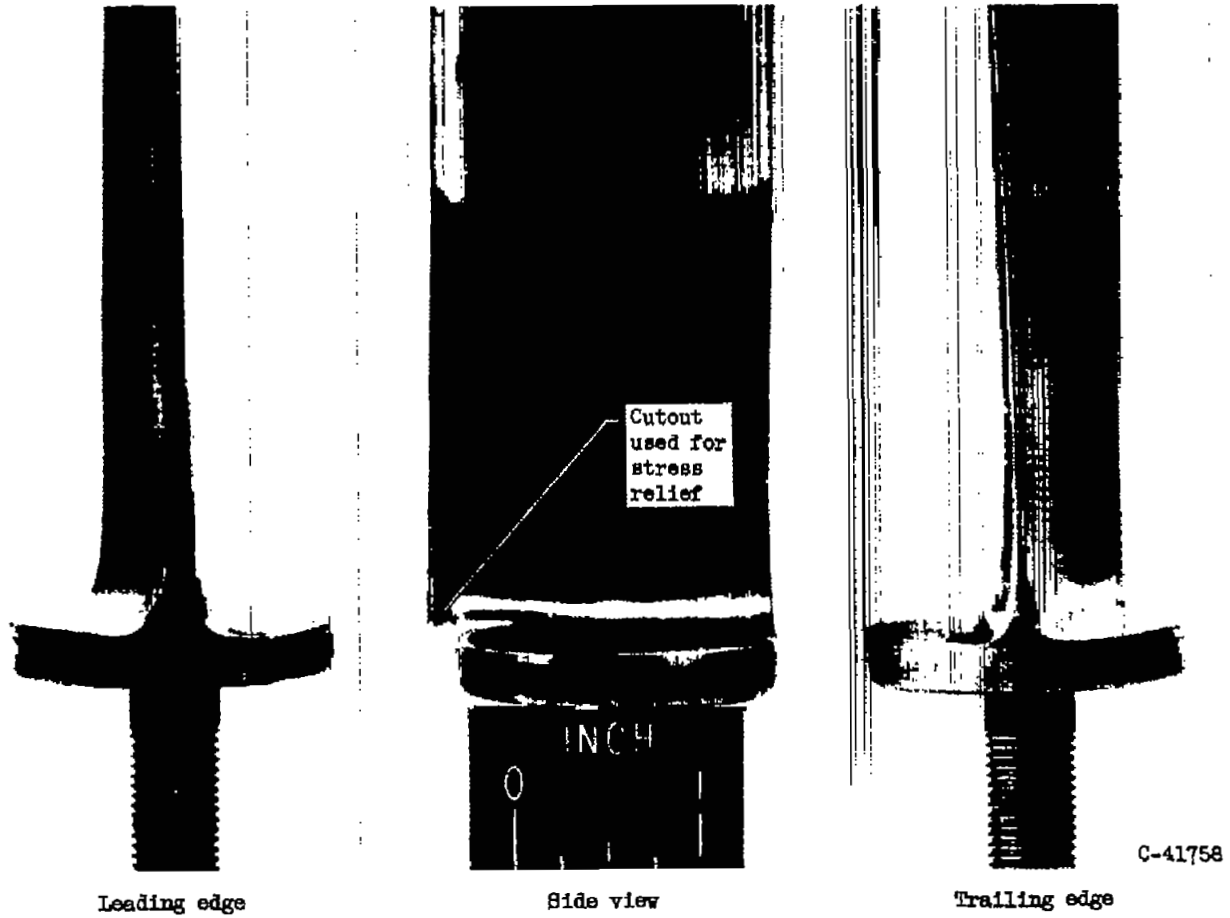
(d) Second stator.

Figure 12. - Concluded. Stator and rotor blade row airfoil-section characteristics.



(a) First spool.

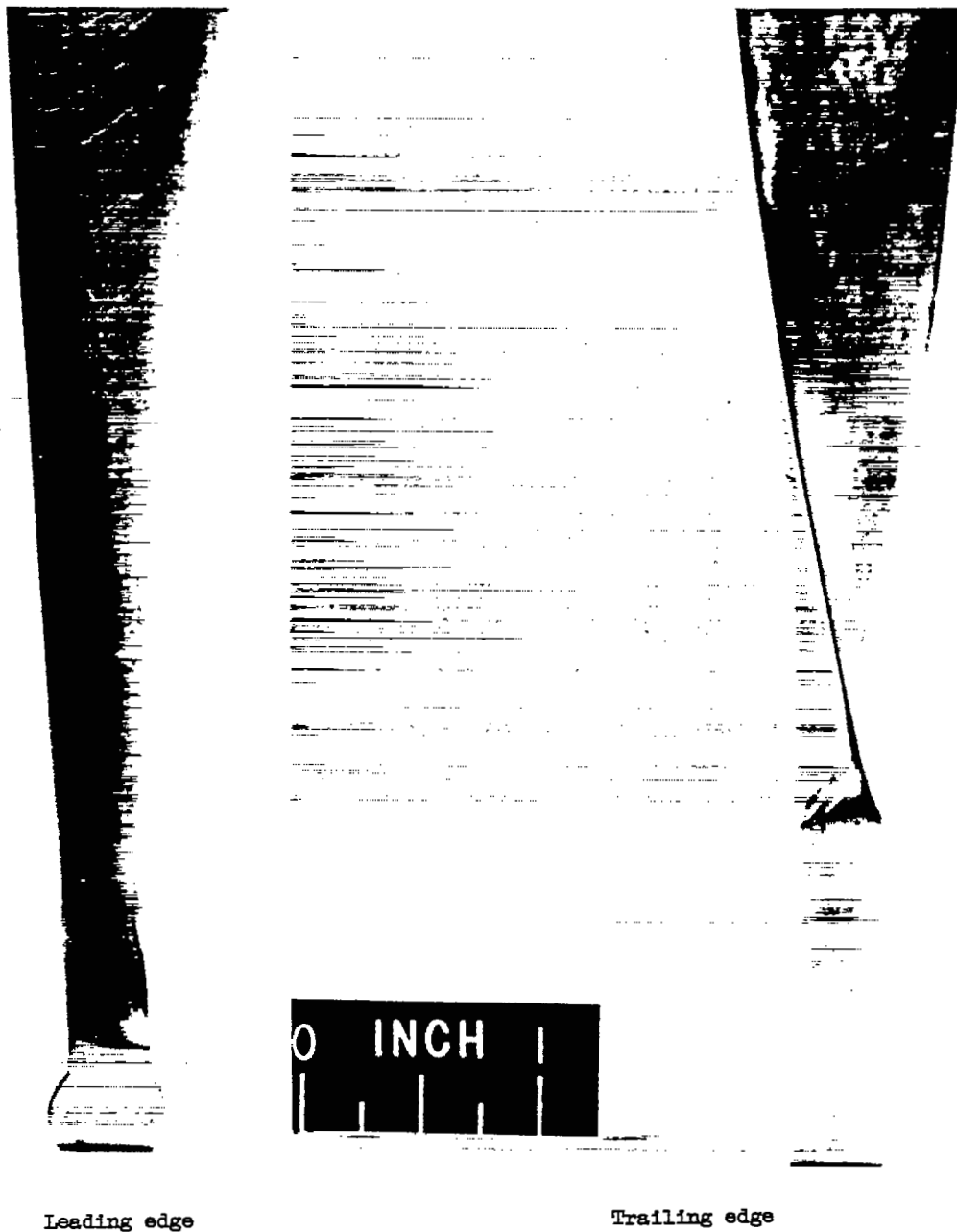
Figure 13. - Photographs of compressor.



(b) Stator blade.

Figure 13. - Continued. Photographs of compressor.

4288



C-41759

Leading edge

Trailing edge

(c) Rotor blade.

Figure 13. - Concluded. Photographs of compressor.

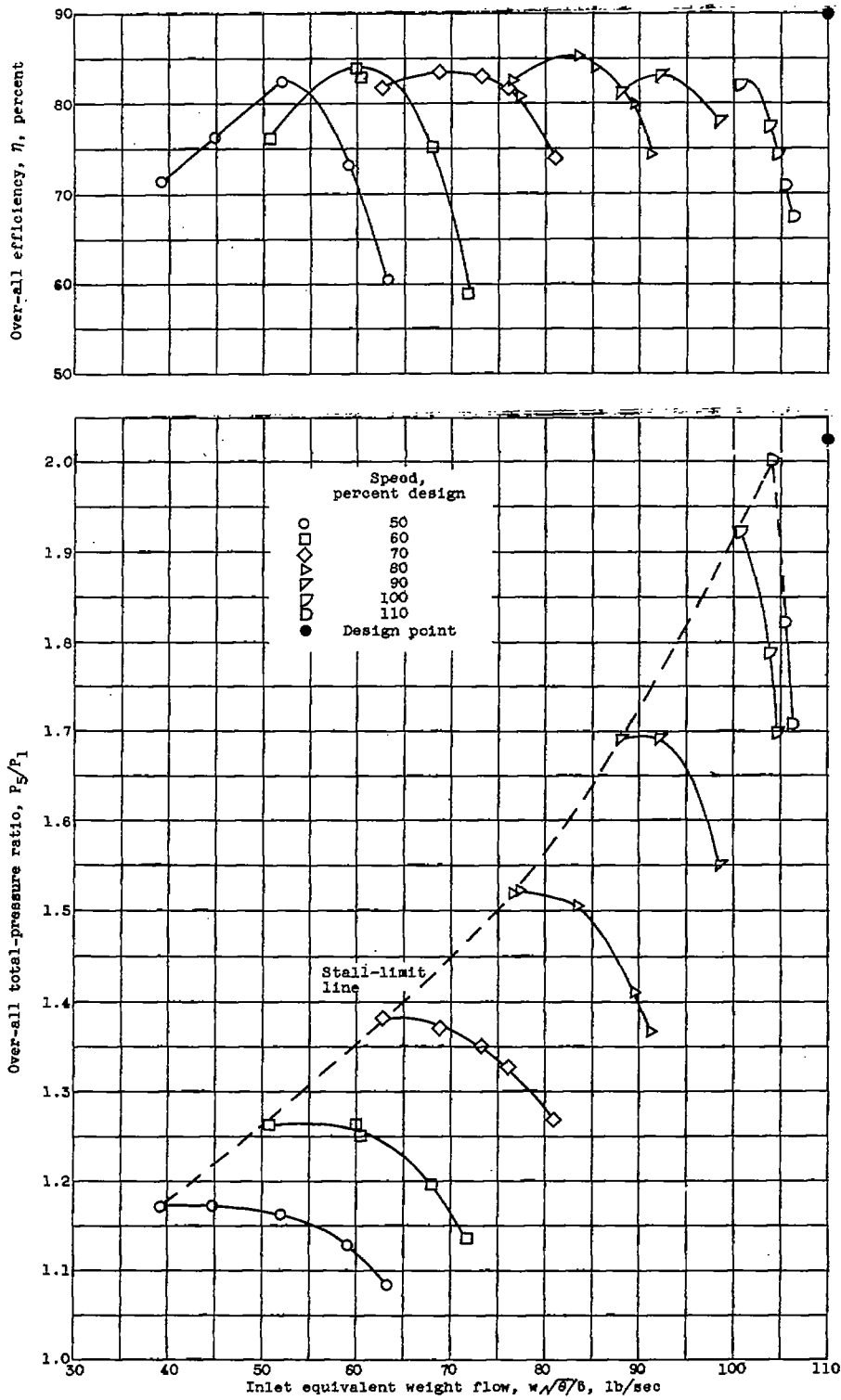
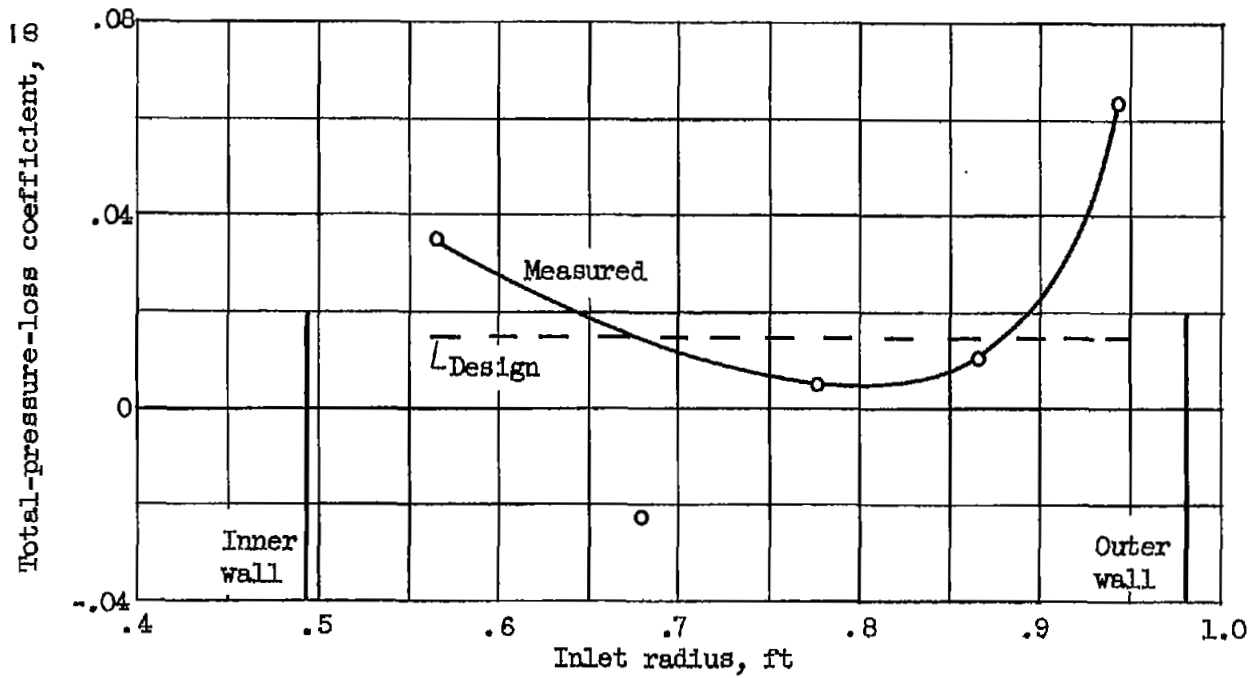
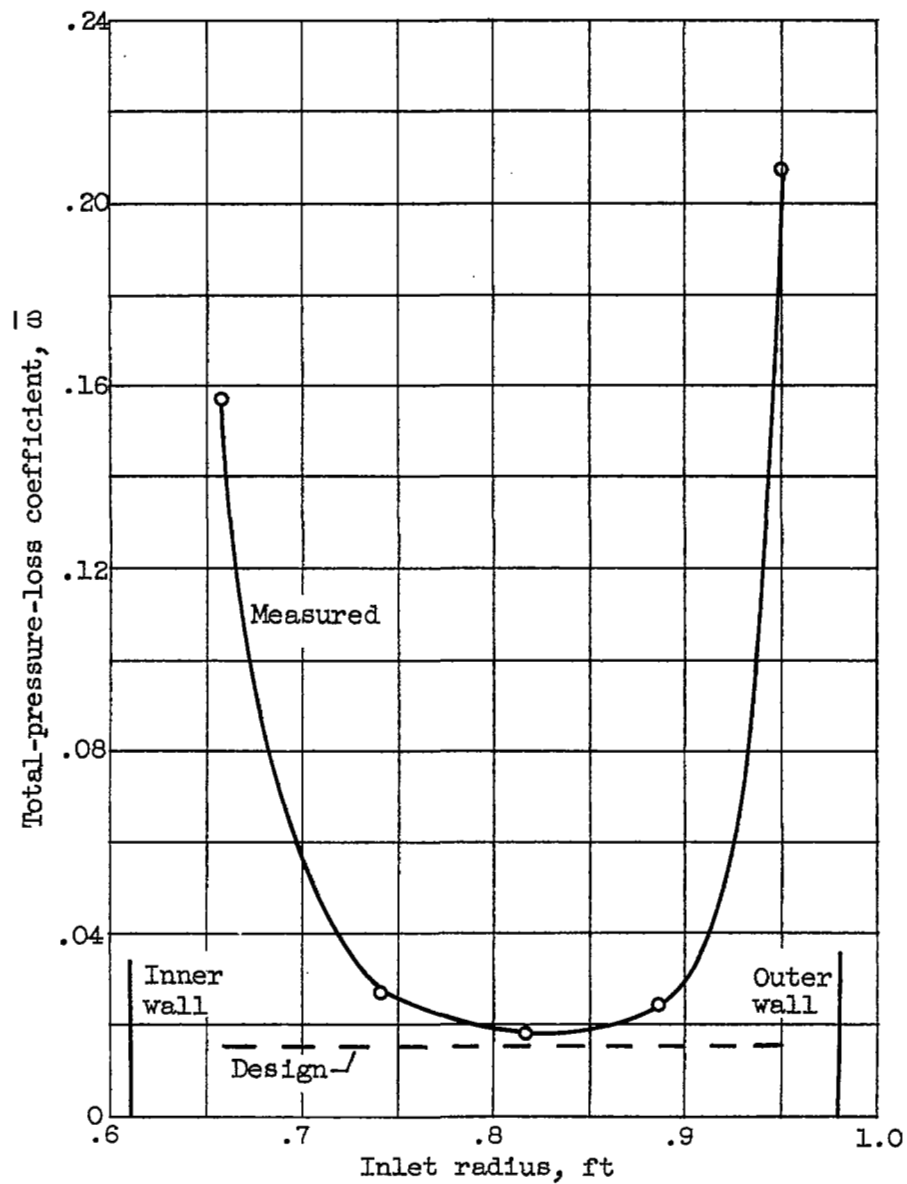


Figure 14. - First-spool over-all performance.



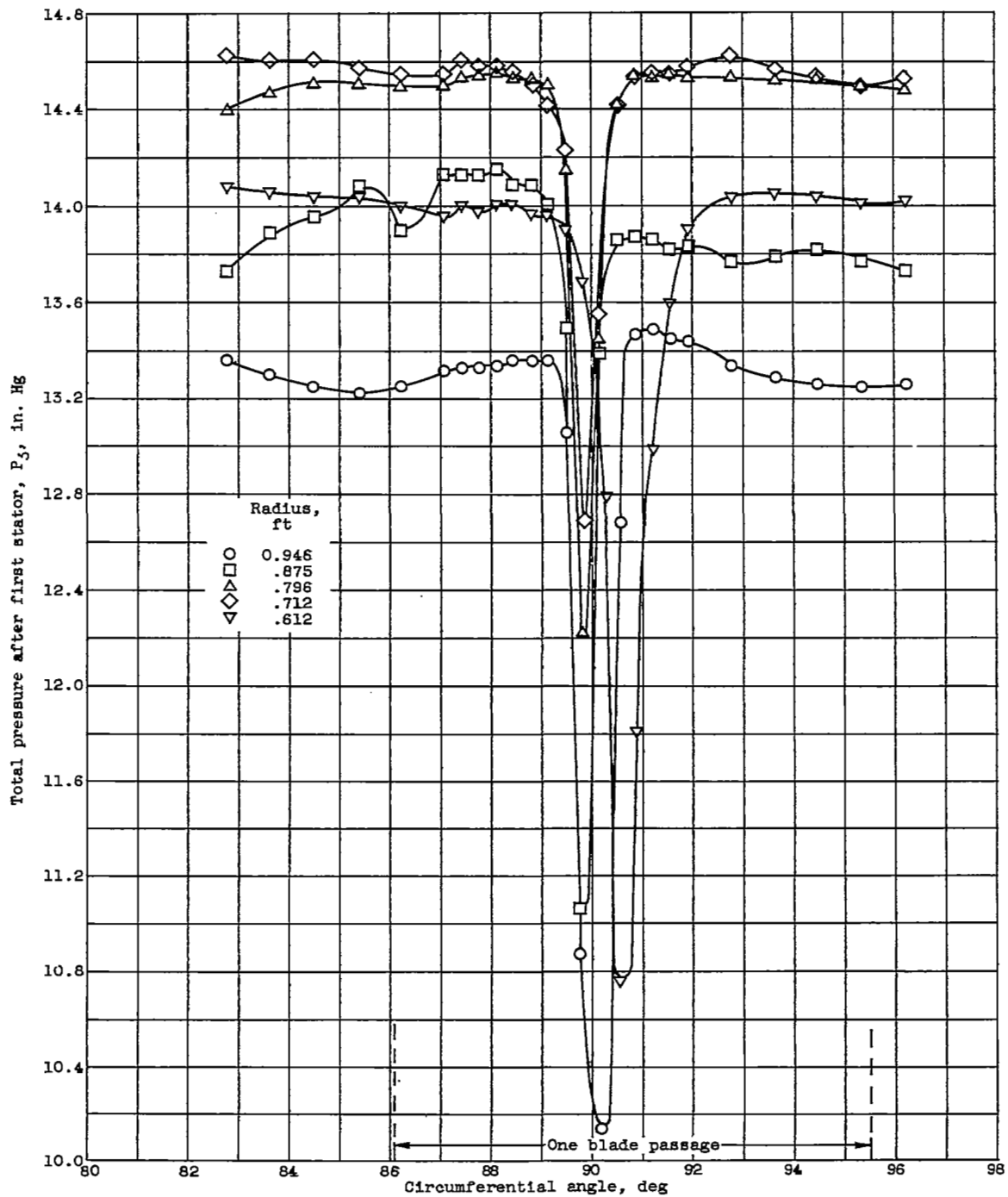
(a) First stator.

Figure 15. - Stator loss coefficient at design speed plotted against radius.



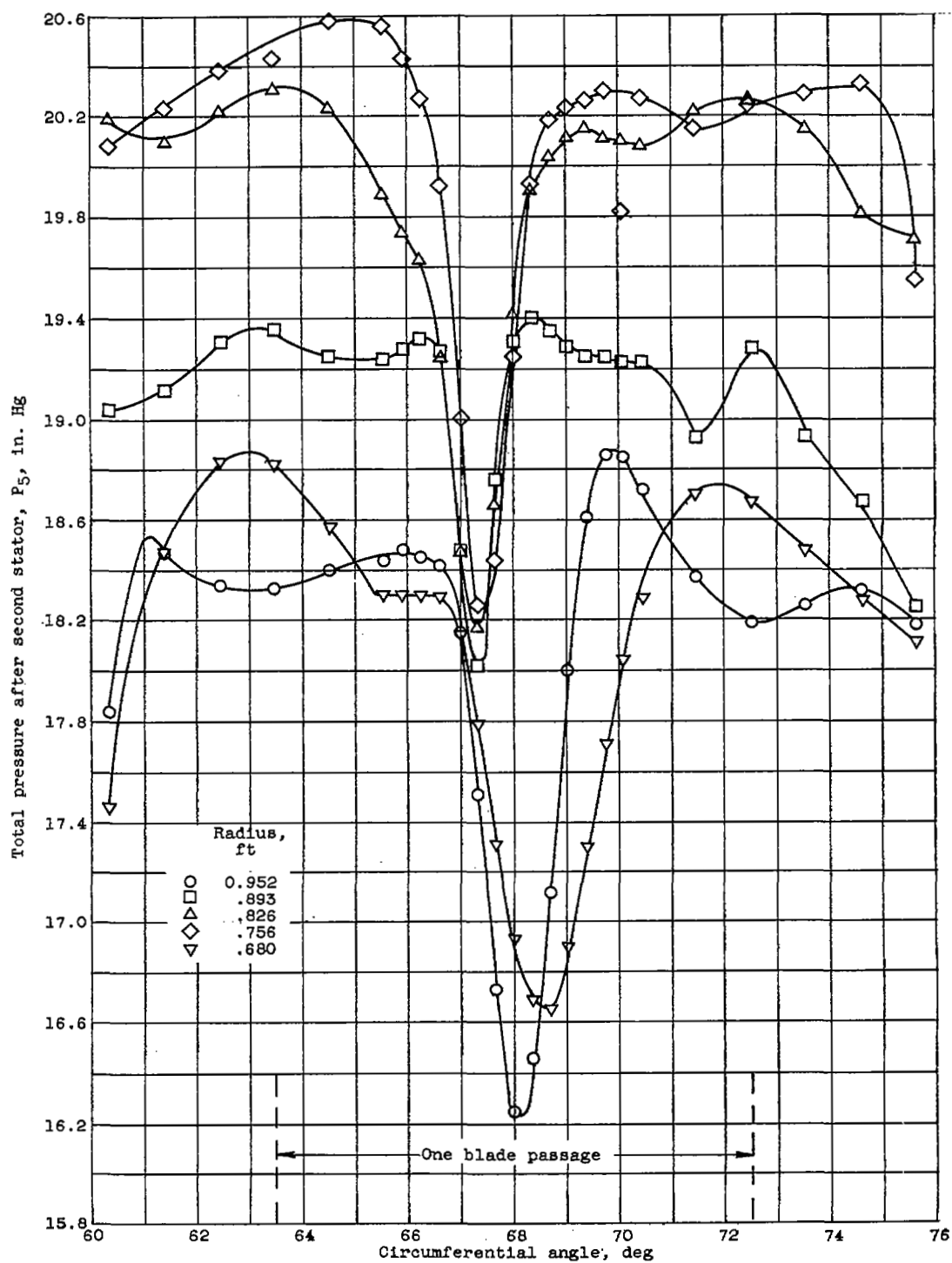
(b) Second stator.

Figure 15.- Concluded. Stator loss coefficient at design speed plotted against radius.



(a) First stator.

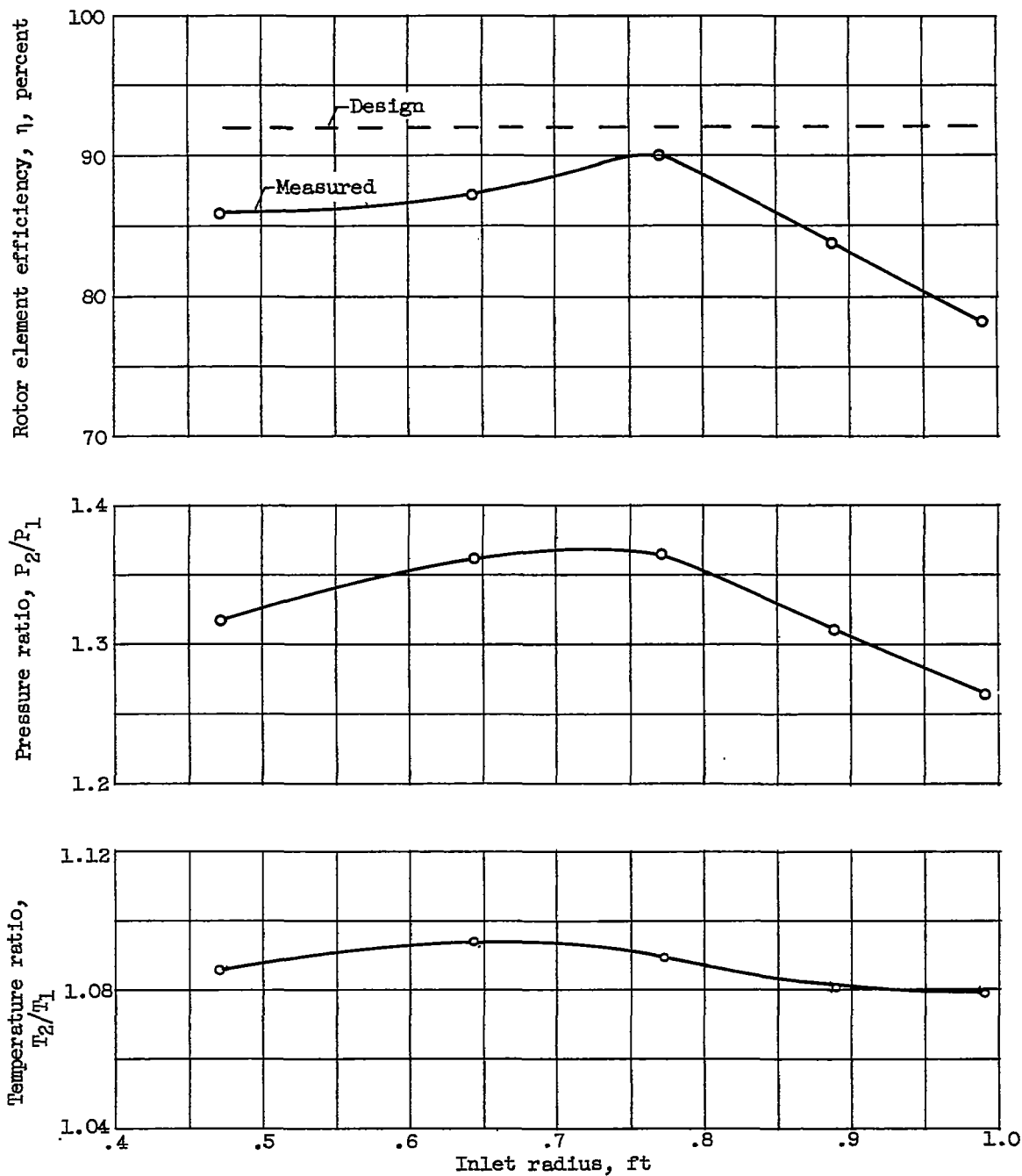
Figure 16. - Total-pressure distribution after stator at design speed.



(b) Second stator.

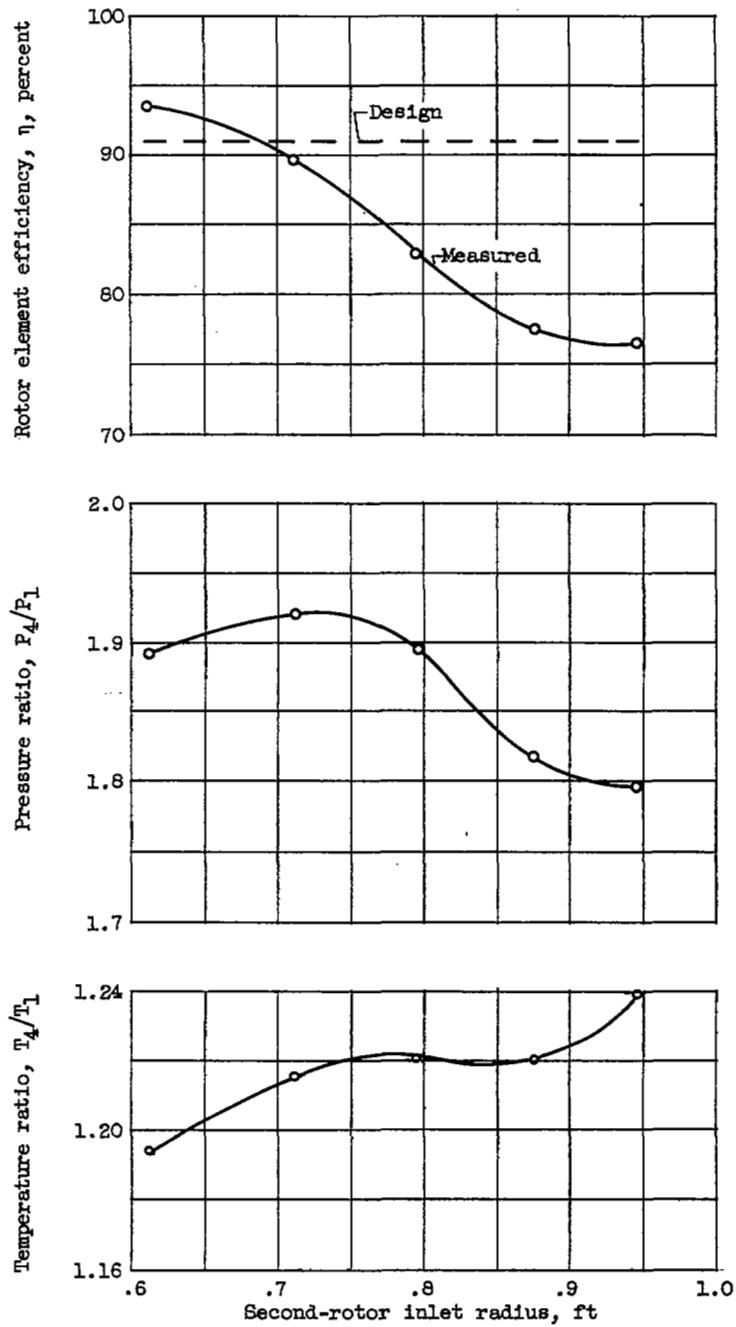
Figure 16. - Concluded. Total-pressure distribution after stator at design speed.

4288



(a) First rotor.

Figure 17. - Radial variation of element efficiency and temperature and pressure ratios at design speed. Inlet temperature, 524° R; inlet pressure, 10.55 inches of mercury absolute.



(b) Second rotor.

Figure 17. - Concluded. Radial variation of element efficiency and temperature and pressure ratios at design speed. Inlet temperature, 524°R ; inlet pressure, 10.55 inches of mercury absolute.

4288

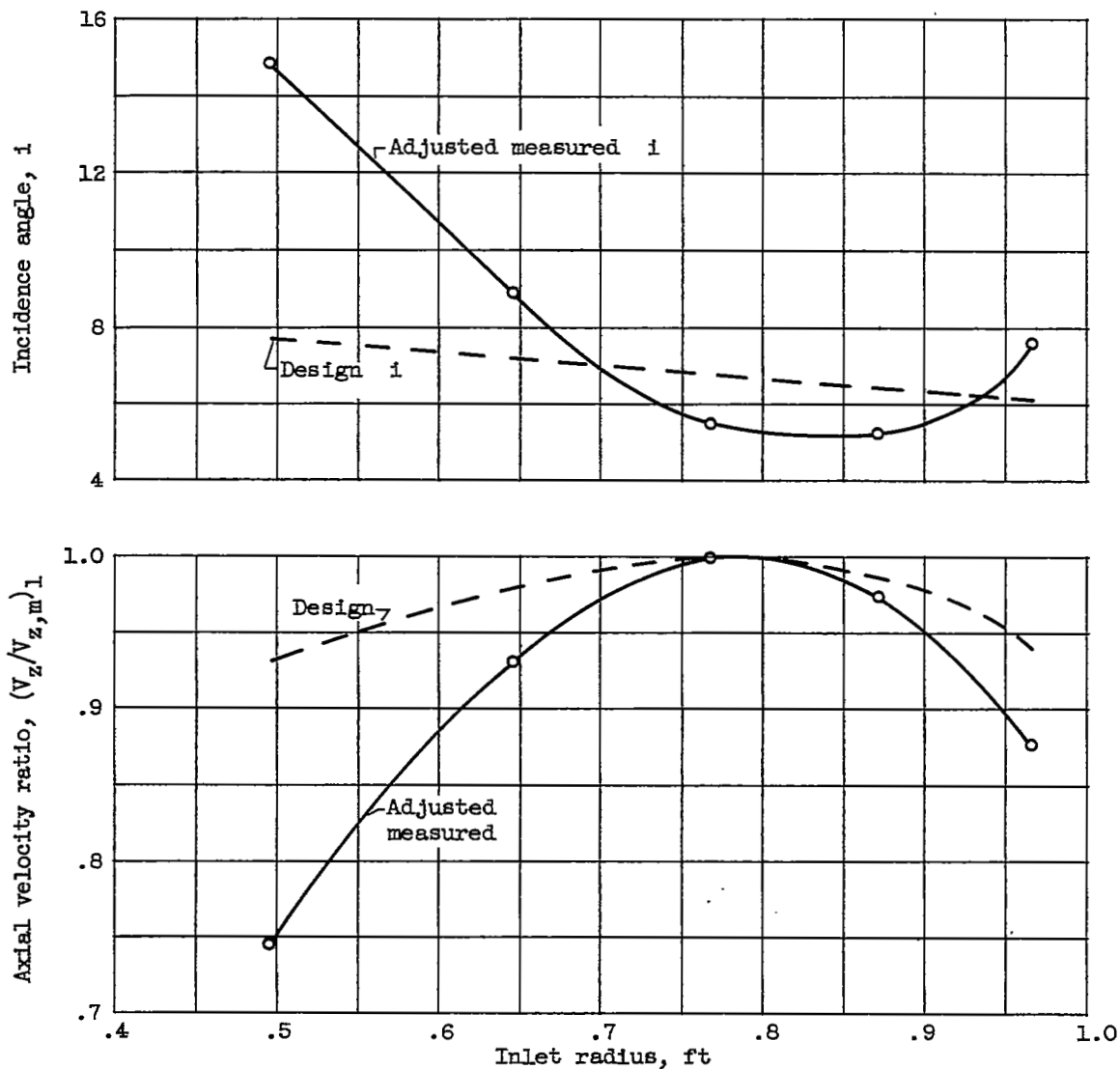


Figure 18. - Comparison of design and measured values of incidence angle and axial velocity distribution at inlet to first rotor. Mean axial velocity at inlet (design), 658; mean axial velocity at inlet (adjusted measured), 694.

NASA Technical Library



3 1176 01436 5556

CONFIDENTIAL